ПРИЛОЗИ. ОДДЕЛЕНИЕ ЗА ТЕХНИЧКИ НАУКИ
CONTRIBUTIONS. SECTION OF TECHNICAL SCIENCES

Прилози. Одд. за тех. науки, МАНУ	Том **XXXVIII**	Бр. 1-2	Стр. 1-60	Скопје 2017
Contributions. Sec. of Tech. Sci., MANU	Vol.	No.	pp.	Skopje

UDC 62 ISSN 1857-6656

МАКЕДОНСКА АКАДЕМИЈА НА НАУКИТЕ И УМЕТНОСТИТЕ
MACEDONIAN ACADEMY OF SCIENCES AND ARTS
ОДДЕЛЕНИЕ ЗА ТЕХНИЧКИ НАУКИ
SECTION OF TEHNICAL SCIENCES

П Р И Л О З И

C O N T R I B U T I O N S

XXXVIII 1-2

СКОПЈЕ - SKOPJE
2018

Прилози, Одд. за тех. науки, МАНУ, XXXVIII, 1–2 (2017) стр, 5–11
Contributions, Sec. Tech. Sci., MANU XXXVIII, 1–2 (2017) pp. 5–11
ISSN 1857–6656
UDC: 061-12(497.7)"1967/2017"(060.91)

ON THE EVE OF THE GREAT JUBILEE – 50 YEARS OF THE MACEDONIAN ACADEMY OF SCIENCES AND ARTS 1967 – 2017

Taki Fiti

President of the Macedonian Academy of Sciences and Arts

This year the Macedonian Academy of Sciences and Arts (MASA) marks and celebrates a great jubilee – 50 years of existence and work of our highest institution in the field of sciences and arts. Although on 22 February 2017 the 50th anniversary of the enactment of MASA in the Assembly of the Socialistic Republic of Macedonia was marked, and on October 10 it will be 50 years since the solemn establishment of MASA, we proudly emphasize that our roots, the roots of the Macedonian and Slavic cultural and spiritual continuity, are far back, in a time dimension which is measured in centuries. Because the mission of the Ss. Cyril and Methodius, the historical events that made Ohrid, with the famous Ohrid Literary School, already in the IX century to become the center of the Slavic educational and enlightening activity, which then spread throughout all Slavic countries, have fundamentally changed our contribution to the treasury of the European culture and civilization. And furthermore, centuries later, in the middle of the XIX century the Macedonian revival began, with a pleiad of our cultural and national activists. These processes at the beginning of the XX century resulted in the establishment of the Macedonian Scientific and Literary Fellowship in Saint Petersburg, led by Dimitrija Chupovski and Krste Petkov Misirkov, whose rich scientific, literary and cultural activities were a significant reflection of our spiritual continuity and identity, and an event that has marked the dawn of the Macedonian Academy of Sciences and Arts. This continuity will remain in the period between the two world wars, with a pleiad of artists

in literature, art, music, philological, economic, legal and technical sciences. A few years after World War II, in 1949, in free Republic of Macedonia, the first state University of "Ss. Cyril and Methodius" was established, within which, in less than two decades, solid personnel resources were created which allowed rapid development of the higher education and scientific activity in our country. It was an event of great importance for the establishment of MASA as the highest institution in the field of sciences and arts.

This millennium pace and continuity in the development of art and scientific thought in our region is an indication and evidence that we are not a nation without its own roots, without its own history, without its own culture, and that the attempts to deny our identity, language, name, no matter where they come from, are residual of the Balkan anachronisms, and essentially speaking, they are absurd and retrograde.

Immediately after the establishment of MASA followed a period of rapid development, diversification and enrichment of its scientific and research activities and artistic work. Almost two decades after the establishment MASA entered the phase of its maturity and has grown and has affirmed as the fundament of the Macedonian science, language, culture and history and as one of the pillars and symbols of the statehood of the Republic of Macedonia.

Today, MASA, according to its integral concept, structure and function, has all the necessary attributes of a modern national academy of European type, and of course, performs the three basic functions typical of the European national academies: creating communication space for confrontation of different views and opinions on important issues in the field of sciences and arts, scientific and research work and advisory role.

The scientific and research activities and artistic work, in fact, constitute the core of the activity of MASA. The number of completed scientific and research projects and projects in the field of arts within MASA is impressive – more than 1,000 projects in the past 50 years. Some of these projects are long-term and are mainly related to the strategic issues of specific national interest, and significant is the number of fundamental and applied research in all fields of science and art represented in the Academy. MASA members in their scientific research increasingly incorporate the international dimension in the work – in the recent years more than 60% of the scientific papers have been published

in international journals, most of which have been published in journals with impact factor; 50% of the papers that have been published in proceedings of scientific and professional meetings are related to meetings held abroad, etc. In addition, the works of our renowned writers and poets, members of MASA, are translated into foreign languages, and their work has found its place in world anthologies. Our prominent painters and sculptors of the older and the younger generation have created and create masterworks that are regularly exhibited at home and abroad. It should be particularly noted that our two research centers – Research Center for Energy and Sustainable Development and the Research Centre for Genetic Engineering and Biotechnology "Georgi D. Efremov", that have gained high reputation in the region and beyond, continue to successfully maintain the attained position. The work of the other research centers also enhances, including the newly established ones, which have begun to work on significant international scientific and research projects.

In its half-century of existence and work MASA developed a rich publishing activity. Since its establishment until today around 700 titles have been published – monographs, results of scientific projects, proceedings from scientific meetings, music releases, facsimile and jubilee publications, joint publications with other academies and scientific institutions, publications of solemn meetings, special issues of the departments of MASA etc. A special contribution to the publishing activities of MASA provides the "Trifun Kostovski" Foundation that has been existing and working for 18 years.

MASA proactively follows the changes and the new trends in the scope of the advisory function of the modern European national economies, and in that context the obligations arising from the project SAPEA - Science Advice for Policy by European Academies, initiated by the European Commission in order to intensify the cooperation of the European academies within their advisory role. Through the publication of the results of our scientific and research work, their presentation to the wider scientific and professional public in the country, to the government officials, etc., MASA participates in the policy-making in the field of sciences and arts and in the overall development of the country. The maintenance of the independence of MASA in carrying out the advisory role is our highest priority and principle.

In the recent years MASA has developed extensive international cooperation that contributes to the affirmation of the Macedonian scien-

tific and artistic work and to the increasing of the reputation of MASA and of the Republic of Macedonia in international scale. Today, our Academy cooperates with more than 30 foreign academies and scientific societies and is a member of 7 international associations of academies. In the recent years the cooperation with the academies from the neighboring countries has been intensified, as well as with the Leibniz Society of Sciences from Berlin, and also, within the so-called Berlin process (Joint Science Conference of Western Balkans Process / Berlin Process) the cooperation with the German National Academy of Sciences – Leopoldina, with the French Academy of Sciences, the academies of Southeast Europe and others.

Due to the results achieved in its work, MASA and its members have won a number of high national and international awards. In the past 50 years, MASA has won around 90 awards and recognitions – charters, plaques, certificates of appreciation, medals and decorations from national and international scientific, educational, artistic and other institutions. Particularly, it should be noted that MASA has been awarded with the high decoration Order of the Republic of Macedonia for the contribution to the development of the scientific and research activity and artistic creativity of importance to the development and affirmation of the Macedonian science and state, which is awarded by the President of the Republic of Macedonia, as well as the prestigious Samuel Mitja Rapoport award of the Leibniz Society of Sciences from Berlin, which, for the first time, has been awarded to MASA. Today, 22 members of MASA have the status of foreign, corresponding and honorary members, as well as holders of honorary PhDs at around 60 foreign academies, scientific societies and universities.

***

The developmental trajectory of MASA unambiguously confirms that the Academy, in its 50 years of existence and work, faced with periods of heights, but also periods of descents and turbulences that are most directly linked to the situation in the Macedonian society, i.e. with crisis periods of different nature – the dissolution of the former common state (SFR Yugoslavia), problems with the recognition of the international status of the country after its independence, the embargoes and the blockades of the country in the early transition years, the internal conflict in 2001 and the political crisis in the last two-three years. In such crises

and tense periods the criticism for the Academy grew – that MASA is an institution closed in itself, that MASA stays away from the current issues and developments in the country, and so on. On the one hand, it is a result of the insufficient understanding of the social role of the Academy – MASA is the highest scientific institution, where hasty reactions of columnist 'type', with daily political features are not characteristic. On the contrary, MASA uses facts and arguments. The basic activity of MASA, the results achieved in the scientific research and the artistic work is our identification within the national and international professional and scientific community, and beyond, within our society. On the other hand, this criticism and perception of MASA has a real basis in the fact that MASA, as opposed to the huge opus of implemented scientific and research and artistic projects still insufficiently affirms the results of its scientific and artistic production to the public. It is our weakness that we must overcome in the future. Of course, we cannot and must not "turn a blind eye" to the other weaknesses and omissions which, at least from time to time, we have faced with over the past 50 years and which we will face with in the future – insufficient scientific criticism of the events in the field of sciences and arts, insufficient resistance to political influence etc. On the contrary, in the future, we will have to clearly identify the weaknesses and the oversights in our work and to find out the right approaches to overcome them.

Today we live in a world of great science. The strong development of sciences, the new technological model based on information and communication technologies, the new wave of entrepreneurial restructuring of economies and societies, the globalization of the world economic activity, opened new perspectives to the economic growth and the development of individual countries and of the world economy as a whole. However, these processes, by their nature, are contradictory. The latest global financial and economic crisis of 2007-2009 revealed the contradictions of the globalization and the discontent of the people from it – the uneven distribution of wealth and power among individual countries, destruction of the resources and the environment worldwide, exhaustion of power of the existing technology and development models. These processes resulted in other problems – refugee and migration crises, strengthening of the regional and national protectionism despite the efforts to liberalize the international trade, fencing of the countries with walls at

the beginning of the new millennium, changes in the economic and technological power and of the geo-strategic position and importance of entire regions and continents, etc. Nevertheless, one thing is a fact – societies that aspire to grow into societies and knowledge-based economies more easily deal with all the above mentioned problems, challenges and risks of the modern world. Of course, moving towards a development knowledge-based model assumes large investments of resources in education, science, research and development and in culture, simultaneously accompanied by well-conceived and devised strategies on development of these crucial areas of the human spirit and civilizational endurance. Hence, this fact, undoubtedly, emphasizes the special significance of the national academies of sciences and arts in achieving this objective.

In the recent years the Republic of Macedonia has been facing with the most difficult political and social crisis in the period after its independence. We are facing a crisis of the institutions, breach of the principles of the rule of law, the phenomenon of "captured state", a decline in the process of democratization of the society and falling behind on the road to the Euro-Atlantic integration processes. The problems that are now in the focus of our reality will require major reforms, much knowledge, energy and political will to overcome them. In this sense, and in this context, the role of MASA and of the overall scientific potential of the country in overcoming the crisis is also particularly important.

The above summarized evaluations and considerations about the development of MASA in the past 50 years, about the achievements in the realization of its basic activity, about the problems it faced and faces with, about the major challenges arising from the new age and which are determined with the changes in the international and national environment, they alone define the main priorities of our Academy in the forthcoming period:

- Our long-term goals are contained in the mission and vision of MASA as the highest institution in the field of sciences and arts. The mission of MASA is through the development of the basic functions that are characteristic for all modern national academies of European type, to give its full contribution to the inclusion of the Macedonian science and art in the modern European and world trends, and our vision is the Republic of Macedonia to become an advanced society based on science and knowledge;

- In the forthcoming years the focus of the scientific and research activity and artistic work of MASA, in cooperation with the other scientific and research institutions in the country and with government experts, will be particularly focused on the elaboration of issues and topics that are most directly related to the sources of the current political and social crisis in the country in order to offer possible solutions, approaches and policies to overcome it;

- The issues related to the Euro-Atlantic integration processes of the Republic of Macedonia, their continuous and persistent scientific monitoring and elaboration and active participation of MASA members in the preparation for the accession negotiations with the EU will remain a high priority on the agenda of MASA. Our ultimate goal is the Republic of Macedonia to become a democratic, economically prosperous and multicultural European country.

- The increasing incorporation of the international dimension in the scientific and artistic work of MASA, through the cooperation with foreign academies, scientific societies and other scientific institutions, through application and work on scientific projects financed by the European funds and the funds of other international financial institutions, also remains our important priority.

Let us congratulate ourselves on the great jubilee – 50 years of the Macedonian Academy of Sciences and Arts.

Прилози, Одд. за тех. науки, МАНУ, XXXVIII, 1–2 (2017) стр, 13–30
Contributions, Sec. Tech. Sci., MANU XXXVIII, 1–2 (2017) pp. 13–30
ISSN 1857–6656
UDC: 539.184.3/.5:533.92]:[546.291:546.11

ELECTRON CAPTURE, EXCITATION AND IONIZATION PROCESSES IN HE^{2+} – H COLLISIONS IN QUANTUM PLASMAS

R. K. Janev[1] and D. Jakimovski[2]

[1] Macedonian Academy of Sciences and Arts, P.O. Box 428, 1000 Skopje, Macedonia
[2] Department of Physics, Sts Cyril and Methoduius University, P.O. Box 162, 1000 Skopje, Macedonia

Abstract: Electron capture, excitation and ionization processes in He^{2+}- H collisions taking place in quantum plasmas are studied by employing the two-center atomic orbital close coupling (TC-AOCC) method. The Debye-Hückel-cosine (DHC) potential is used to describe the plasma screening effects on the Coulomb interaction between charged particles. The properties of eigenenergies of hydrogen-like atom with DHC potential are investigated as function of the screening length of the potential. It is found that the binding energies of *nl* states decrease with decreasing the screening length of the potential. The dynamics of excitation, electron capture and ionization processes in He^{2+}- H collision system is investigated when the screening length of the potential varies for a wide collision energy range. The TC-AOCC cross sections are compared with those for the pure Coulomb potential and, for the total electron capture, with the results of classical trajectory Monte Carlo (CTMC) method.

I. INTRODUCTION

The plasma screening effects on the atomic structure and radiative and collision processes taking place in a plasma environment have been sub-

ject to extensive studies in last several decades. Most of these studies have been performed for the weakly coupled classical plasmas in which the interaction between charged plasma particles is described by the well-known Debye-Hückel potential $V(r) = -Ze^2 \exp(-r/\lambda)/r$ [1], where Ze is the positive ion charge e is the elementary charge and $\lambda = (k_B T_e / 4\pi n_e^3)^{1/2}$ is the Debye length with T_e, n_e, k_B being the lectron plasma temperature, density and the Boltzmann constant. The validity of Debye-Hückel potential for describing the screened interaction in a weakly coupled classical plasma requires the condition $\lambda \geq \bar{a} = \left(3/4\pi n_e\right)^{1/3}$, where $\bar{a}$ is the average interparticle distance.

Many theoretical studies of electronic structure and radiative properties of one-electron atomic systems and their electron, photon and ion-impact collision processes have been performed in weakly coupled plasmas using Debye-Hückel potential and reviewed recently [2]. In plasmas with temperatures lower than the electron Fermi temperature T_F $(= \hbar^2 \left(3\pi^2\right)^{2/3} n^{2/3} \big/ 2m)$ ($\hbar$ being the reduced Planck constant) and densities such that de Broglie wavelength λ_B $(= \hbar / mv_{th})$ (v_{th} is the thermal velocity, m is the electron mass) satisfies the condition $\lambda_B \geq \bar{a}$, the quantum effects (quantum tunneling, quantum diffraction, etc.) start to become important (quantum plasmas). Quantum plasmas are observed in metals, nanoscale structures, semiconductor devices and in compact astrophysical objects (e.g. neutron stars, white dwarfs). The interaction between a positive charge Ze and an electron in such plasmas has the form [3]

$$V(r) = -\frac{Ze^2}{r} \exp(-r/\kappa) \cos(r/\kappa) \tag{1}$$

where $\kappa = 2^{1/2} / k_q$ and $k_q = \left(4m^2\omega_p^2 / \hbar^2\right)^{1/4}$ is the electron quantum wavenumber and $\omega_p = (4\pi e^2 n_e / m)^{1/2}$ is the plasma frequency . We note that for infinitely large screening length κ the potential (1) reduces to the pure Coulomb potential.

Atomic structure properties and collision processes in quantum plasmas involving the potential (1) have received a considerable attention in recent years [4-15].

In particular, the electron capture process in H^++H collisions has been studied in Refs. [11] and [14] by employing the CTMC and TC-AOCC methods, respectively. The CTMC method was also used to study the electron capture in He^{2+}+H collisions. In the present work we shall study the dynamics of excitation, electron capture and ionization processes in He^{2+}+H collisions taking place in a quantum plasma

$$\mathrm{He}^{2+} + \mathrm{H}(1s) \rightarrow \mathrm{He}^{2+} + \mathrm{H}(nl) \quad (2a)$$
$$\rightarrow \mathrm{He}^{+}(nl) + \mathrm{H}^{+} \quad (2b)$$
$$\rightarrow \mathrm{He}^{2+} + \mathrm{H}^{+} + e \quad (2c)$$

by employing the TC-AOCC method with a large expansion basis. We shall examine the structural properties of the hydrogen atom with the potential (1), the dependence of partial (state-selective) cross sections of reactions (2a) and (2b) on the screening length κ and compare them with the results of unscreened Coulomb interaction and, in the case of reaction (2b), with the available total electron capture CTMC result of Ref. [12].

The organization of the article is as follows. In Section II we discuss the properties of eigenenergies of hydrogen atom with the interaction (1). In Section III we shall outline the TC-AOCC computational method used for description of the collision dynamics of reactions (2) and in Section IV we present and discuss our results. Finally, in Section V we give our conclusions.

In the remainder of this paper we shall use atomic units ($\hbar = m = e = a_0 = 1$), unless otherwise explicitly indicated.

II. PROPERTIES OF EIGENENERGIES OF HYDROGEN ATOM WITH THE DHC POTENTIAL (1)

The most important properties of DHC potential (1), that decreases faster than $-1/r^2$ when $r \rightarrow \infty$, are the lifting of degeneracy of angular momentum states and the finite number of bound states supported by the potential for any finite value of the screening length [16]. The latter property

implies that the energies E_{nl} of bound states decrease with decreasing length κ. At certain critical value κ_c^{nl} the binding energy of nl state becomes zero and the state enters the continuum (and remains there for all $\kappa \leq \kappa_c^{nl}$). It should be noted that the radial Schrödinger equation with the potential (1) is scalable with respect to the charge Z [14], so that the energies of a hydrogen-like ion are scaled as $\varepsilon_{nl} = E_{nl}/Z^2$ and screening lengths as $\delta = Z\kappa$ .The scaled energies of the nl ($n \leq 3$) states of a hydrogen-like atom with the potential (1) as function of the scaled screening length δ, calculated by the method described in Section III, are shown in Fig. 1. In Table 1 we give the scaled critical screening lengths δ_c^{nl} for the states with $n \leq 6$. The table shows that for a given value of δ only a finite number of states remain bound in the potential and that the critical screening length increases with increasing the angular momentum quantum number l for a given value of the principal quantum number n.

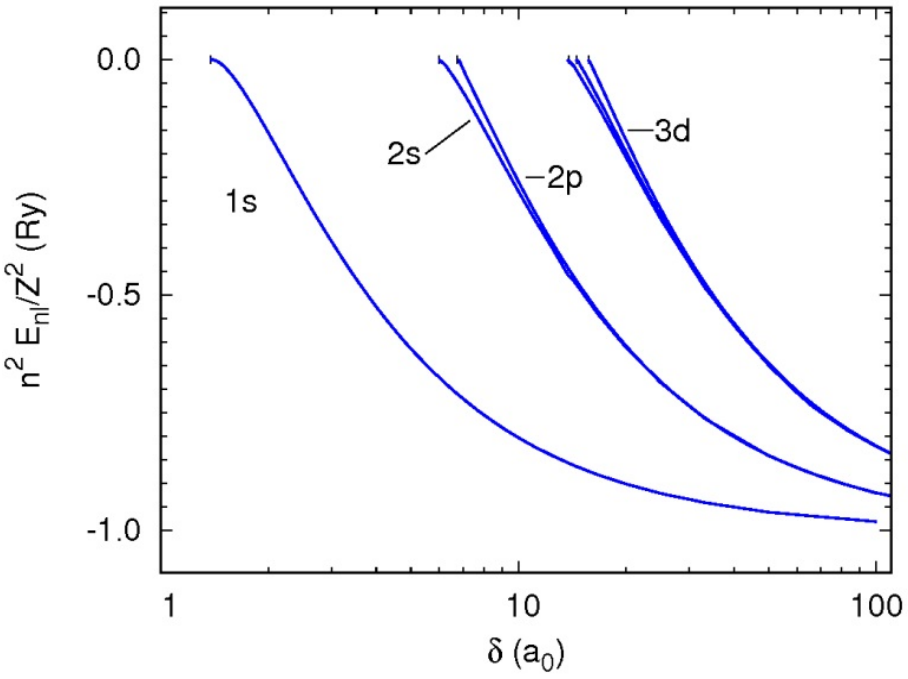

Fig. 1. Scaled energies of 1s, 2l and 3l states of hydrogen-like atom in the potential (1) as function of scaled screening length $\delta = Z\kappa$

Table 1.

Scaled critical screening lengths δ_c^{nl} (in a_0) for $n \leq 6$ states in the potential (1)

$n\backslash l$	0	1	2	3	4	5
1	1.3858					
2	5.9974	6.7474				
3	13.7982	14.5534	15.7278			
4	24.7260	25.4687	26.7343	28.3758		
5	38.7660	39.5007	40.8161	42.5855	44.6999	
6	55.9179	56.6496	57.9944	59.8509	62.1138	64.7020

III. COMPUTATIONAL METHOD

For calculation of the cross sections of reactions (2) we shall employ the TC-AOCC method, described in detail elsewhere [17, 18]. The total scattering wave function in this method is expanded in terms of electronic states centered on both centers. For determining the bound electronic states with the potential (1) on either of the two centers, one uses the variational method with even-tempered trial functions [19]

$$\chi_{klm}(\vec{r};\delta) = N_l(\xi_k(\delta))r^l e^{-\xi_k(\delta)r} Y_{lm}(\hat{\vec{r}}) \qquad (3)$$
$$\xi_k(\delta) = \alpha\beta^k, \quad k = 1,2,....N$$

where $N_l(\xi_k)$ is a normalization constant, $Y_{lm}(\mathbf{r})$ are the spherical harmonics and α and β are variational parameters, determined by minimization of the energy for each value of the screening length κ_D. The atomic states $\phi_{nlm}(\vec{r};\delta)$ are then obtained as linear combinations

$$\phi_{nlm}(\vec{r};\delta) = \sum_k c_{nk}\chi_{klm}(\vec{r};\delta) \qquad (4)$$

where the coefficients c_{nk} are determined by diagonalization of single-center Hamiltonian. This diagonalization yields the energies $\varepsilon_{nl}(\delta)$ of the bound states in the DHC potential (1). In order to describe the ionization process, one needs to include in the expansion basis (4) also states with positive energies (pseudostates) centered on either of the centers. It is

natural to place them on the target, since the dominant part of ejected electron distribution is expected to be around the target.

The total electron wave function Ψ is expanded in terms of atomic orbitals (4) centered on the target (T) and projectile (P) (each orbital multiplied by a plane wave electron translational factor to satisfy the boundary conditions) [17, 18]

$$\Psi(\vec{r},t;\kappa) = \sum_i a_i(t)\phi_i^T(\vec{r},t;\kappa) + \sum_j b_j(t)\phi_j^P(\vec{r},t;2\kappa) \tag{5}$$

in which the basis $\{\phi_i^T(\vec{r},t;\kappa)\}$ includes also the wave functions of continuum pseudostates (we denote them by $\tilde{\phi}_i^T(\vec{r},t;\kappa)$ and their amplitudes by $\tilde{a}_i(t)$). In the second term of Eq. (5) the argument of the traveling orbital contains the screening length $\delta = Z\kappa = 2\kappa$ because the projectile has charge Z=2. While, as mentioned earlier, the wave functions and energies of one-electron systems H and He^+ can be scaled, in the collision problem involving the different target and projectile potentials (see below) they have to be used in unscaled form.

By inserting Eq. (5) it in the time dependent Schrödinger equation $i\partial\Psi/\partial t = H\Psi$, where $H = -\nabla_r^2/2 + V^T(r_T) + V^P(r_P)$ and $V^{T,P}(r_{T,P})$ have the form of Eq. (1), one obtains the coupled equations for the amplitudes $a_i(t)$ and $b_j(t)$ [17, 18]

$$i(\dot{A} + S\dot{B}) = HA + KB \tag{6a}$$

$$i(\dot{B} + S^{\dagger}\dot{A}) = \bar{K}A + \bar{H}B \tag{6b}$$

where A and B are the vectors of the amplitudes a_i(t) and b_j(t), respectively. S is the overlap matrix ($S^{\dagger}$ is its transposed form), H and $\bar{H}$ are direct coupling matrices involving the states on the target and projectile, respectively, and K and $\bar{K}$ are the *i-j* and *j-i* electron exchange matrices. The solutions of the system of equations (6), under the initial conditions $a_i(-\infty)=\delta_{1i}$, $b_i(-\infty)= 0$, with a rectilinear trajectory for the nuclear motion,

yield for the $1\rightarrow i$ excitation and $1\rightarrow j$ charge exchange cross sections the following expressions

$$\sigma_{ex,i} = 2\pi \int_0^\infty |a_i(\infty)|^2 bdb \tag{7a}$$

$$\sigma_{cx,j} = 2\pi \int_0^\infty |b_j(\infty)|^2 bdb \tag{7b}$$

where b is the impact parameter. The ionization cross section is given by

$$\sigma_{ion} = \sum_i 2\pi \int_0^\infty |\tilde{a}_i(\infty)|^2 bdb\,. \tag{7c}$$

In solving the coupled equations (6) we have used an expansion basis containing all bound states on He^+ with principal quantum number $n \leq 5$ (in total 35), and on the target we have used all bound states with $n \leq 6$ plus the 7*s* bound state . In addition, in the basis centered on H we have included 117 positive energy pseudostates, making the total of 174 states centered on H. This basis was also used in the calculations of excitation, electron capture and ionization processes in He^{2+}+H collisions in the plasma free (pure Coulomb interaction) case in Ref. [20]. By comparing the results of present calculations for different screening lengths with those of Ref. [20] we can see the plasma screening effects of the Coulomb interaction on the cross sections of considered processes.

IV. RESULTS AND DISCUSSION

A. EXCITATION

We first consider the dependence of cross sections for excitation to 2*l* and 3*l* states of H on the scaled screening length κ for two typical collision energies of 25keV/u and 100keV/u. (We note that for the H spectrum, $\kappa = \delta$). The results are shown in panels (a) and (b) of Fig. 2, respectively. It is observed that for both energies the cross section for excitation to the 2*p* state is considerably larger than for the other states for all

values of the screening length, resulting from the dipole character of $1s \rightarrow 2p$ transition. It should be remarked, however, that the $2p$ cross section for E=25keV/u exhibits a maximum at $\kappa \approx 9a_0$, after which it slowly decreases with increasing κ towards its limiting value at $\kappa = \infty$ (plasma free case). In contrast, the $2p$ excitation cross section for E =100keV/u, after its sharp increase at κ slightly above the critical screening length κ_{2p}^{c}, slowly increases with increasing κ. The $2s$ excitation cross section for both energies shows a mild increase with increasing κ. All $3l$ excitation cross sections, after leaving the neighborhood of the critical screening lengths κ_{3l}^{c}, quickly reach a plateau.

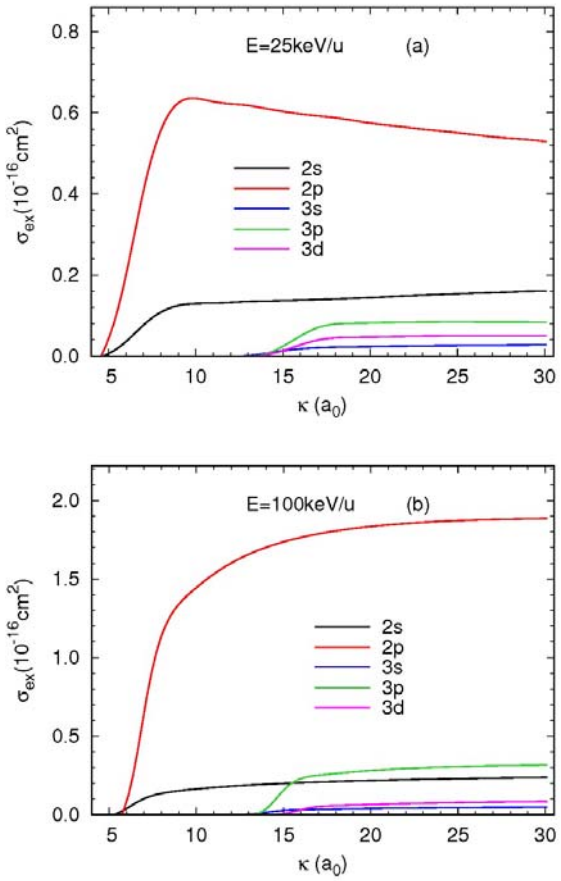

Fig. 2. Dependence of the $2l$ and $3l$ excitation cross sections on the screening length κ for the collision energies of 25keV/u (a) and 100keV/u (b)

In Fig. 3 we show the energy dependence of the 2*s* (panel(a)) and 2*p* (panel (b)) excitation cross sections for the screening lengths κ = 10, 25 and 50a_0 in the interval ~15 – 600keV/u, together with the results for the unscreened Coulomb potential performed in the present work and the results of Kuang and Lin [20]. It can be observed in the figures that the energy dependences of 2*s* and 2*p* excitation cross sections for different values of κ are somewhat different. The 2s cross section for a given value of κ is always smaller than the pure Coulomb cross section in the energy region above ~20keV/u, it increases with increasing κ and for κ =50a_0 it approaches the cross section with pure Coulomb interaction. In contrast, the 2*p* cross section in the region below ~50keV/u increases with decreasing κ, but above this energy it decreases with decreasing κ. This behavior of 2*s* and 2*p* excitation cross sections is consistent with their κ-dependences in Fig. 2. The physical origin of this difference lies in the difference of the radial electron distributions of 2*s* (more compact) and 2*p* (more diffused) states. At high collision energies the excitation process involves the inner parts of these distributions whose dependence on κ is similar (both decrease with increasing κ), while at low collision energies the asymptotic parts of these distributions for which the more diffused 2*p* distribution shows a much faster increase with decreasing κ than that for 2*s* (see [14]).

Fig. 3 shows that the 2*s* and 2*p* excitation cross sections, calculated in the present work for the pure Coulomb case (full black lines) coincide with the plasma-free results of Kuang and Lin [20] (symbols).

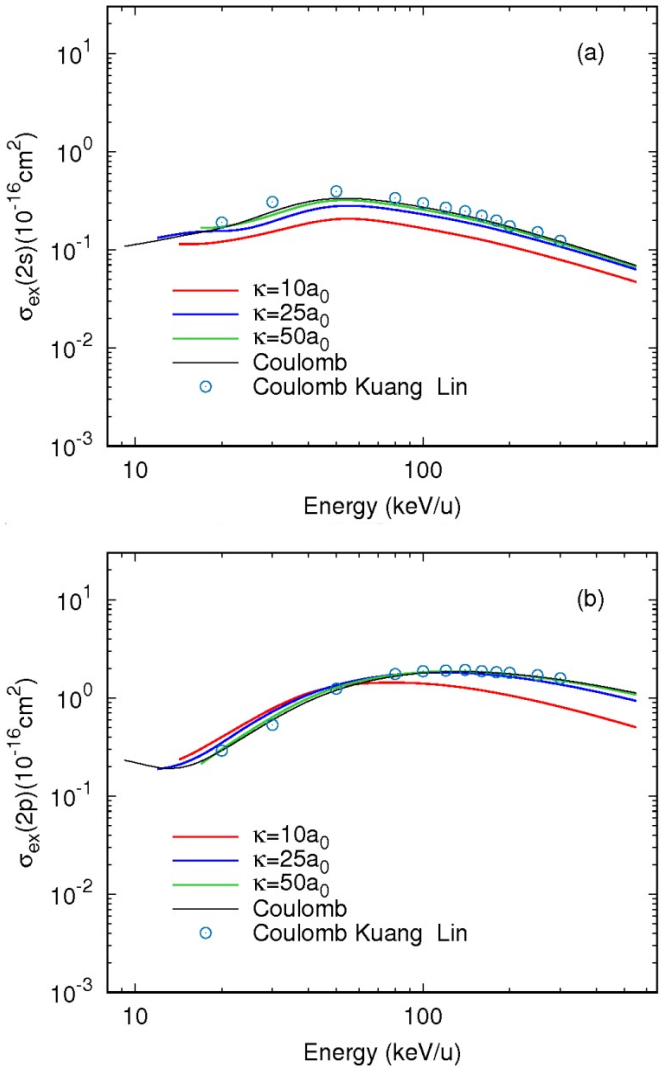

Fig. 3. Energy dependence of 2*s* (a) and 2*p* (b) excitation cross sections for κ = 10, 25, 50a_0 compared with the plasma free cross sections of present calculations (Coulomb) and those of Ref. [20] (Kuang and Lin; symbols)

We have calculated also the cross sections for excitation to 3*l*, 4*l* and 5*l* states for κ = 10, 25, 50a_0. Their values are increasingly smaller than those for the 2*l* states. The summed (very close to the total) cross section is shown in Fig.4, together with that for the pure Coulomb interaction.

The general increase of the excitation cross section with increasing the screening length is due to the fact that for large values of κ increasingly more states remain bound in the potential that can participate in the excitation dynamics.

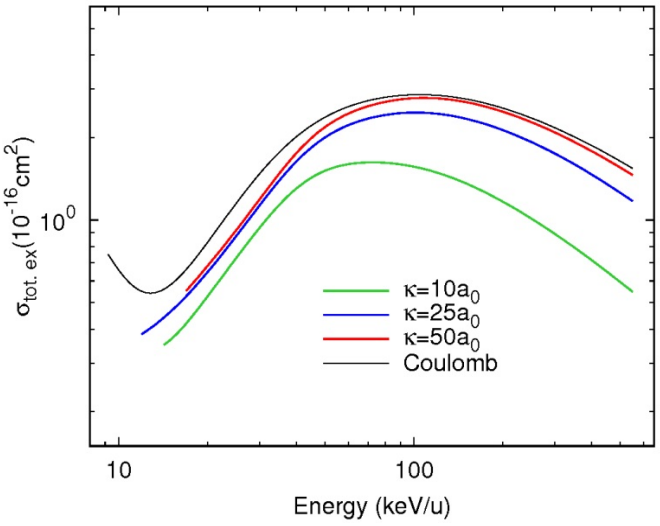

Fig. 4. The total excitation cross section for a plasma with κ = 10, 25, 50a_0 and for the unscreened Coulomb interaction

B. ELECTRON CAPTURE

In Figure 5 we show the κ dependence of 2l and 3l electron capture cross sections for E=25keV/u (panel (a)) and E=100keV/u (panel (b)). The capture states 2l and 3l belong to the He^+ (Z=2) spectrum and the critical screening lengths κ_{nl}^c are now twice smaller than those for the H spectrum, $\kappa_{nl}^c = \delta_{nl}^c/2$ (compare with Fig.2). The capture to 1s state is not included in the panels since its values are negligibly small at all energies due to the large difference between the $He^+(1s)$ and H(1s) energy levels. On the other hand, the H(2l) energy levels are close to the energy of He^+(1s) state for all κ when the H(2l) and $He^+(1s)$ are bound. Fig.5 shows that, like in the case of excitation, for both selected energies the cross section for capture to 2p state of the projectile is larger than for

other transitions. This is a result of the large direct dipole $1s \rightarrow 2p$ coupling of the initial and final states. In all other cases, the population of the final state involves multiple interstate transitions. After the threshold κ_{nl}^{c} the cross section slowly, for E=25keV/u, and much faster, for E=100keV/u, increases with increasing κ and reaches a region of saturation or very slow increase (for $2s$, $3s$ and $3p$ for E=100keV/u). The mild undulations on the $2p$ cross section for E=25keV/u are effects of the κ_{nl}^{c} thresholds of upper states at which they become coupled with the $2p$ state. For the higher energy E=100keV/u these effects are smeared out as the collision time is small.

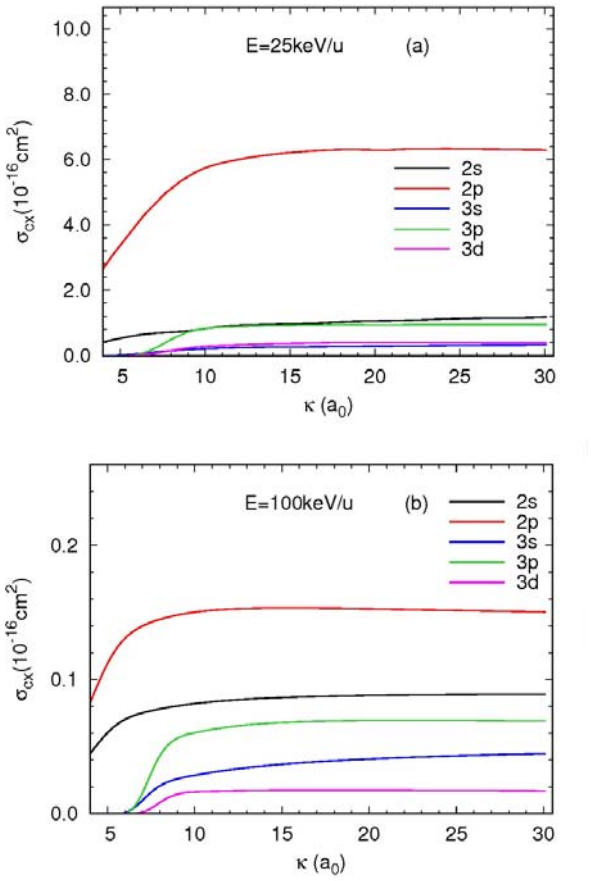

Fig. 5. Dependence on the scaled screening length κ of electron capture cross sections to $2l$ and $3l$ projectile states at E=25keV/u (*a*) and E=100keV/u (*b*)

The energy dependence of dominant electron capture channels to 2*s* and 2*p* projectile states is shown respectively in panels (a) and (b) of Fig.6 in the energy range ~15-300keV/u. Quantum plasmas with screening lengths κ = 5, 10, 25a_0 are selected. The cross sections for capture to these states in the plasma-free case are also shown, including the results of Kuang and Lin [20]. In Fig. 6 we observe that with increasing the screening length κ the 2*s* and 2*p* rapidly increase (somewhat faster for 2*p* and for the higher energies) towards the cross section for the pure Coulomb interaction, with which they coincide already for κ = 25a_0.

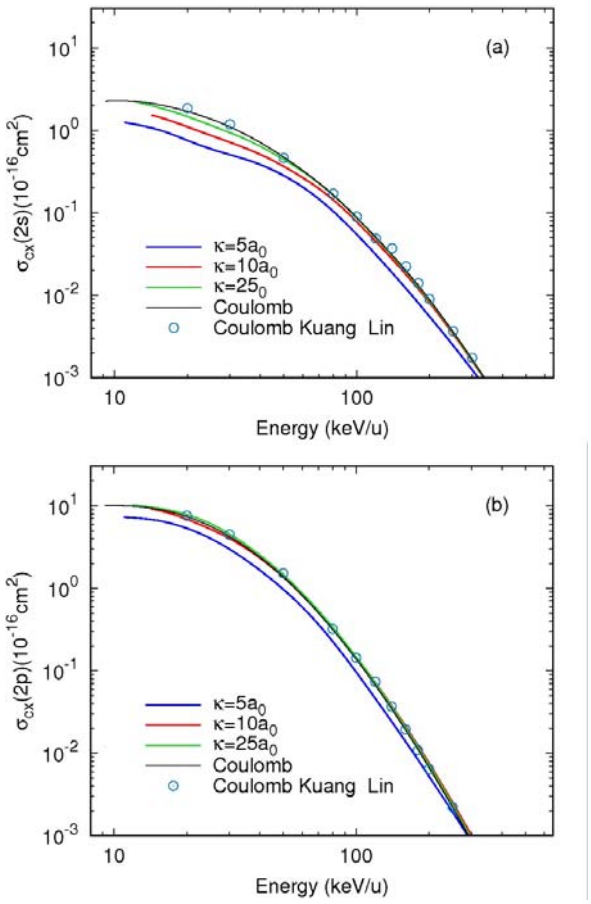

Fig. 6. Energy dependence of cross sections for electron capture to 2s (a) and 2p (b) projectile states for κ = 5, 10, 25a_0 and for the pure Coulomb interaction. The symbols are the results of Ref. [20] for the pure Coulomb interaction case.

We have performed cross section calculations also for capture to 3*l*, 4*l* and 5*l* states for $\kappa = 4.44a_0$ and $\kappa = 10a_0$ and for the pure Coulomb interaction. For these two screening lengths classical -trajectory Monte Carlo (CTMC) calculations with the potential (1) have been performed in Ref. [12]. Our summed (total) cross sections for these two screening lengths are shown in Fig. 7, together with the results of Ref. [12]. The comparison of CTMC and present TC-AOCC results for the two screened potential cases shows that, except for energies below ~30-35keV/u, the CTMC results are larger than the TC-AOCC results. The present result for the pure Coulomb interaction case coincides with the result of Ref. [40].

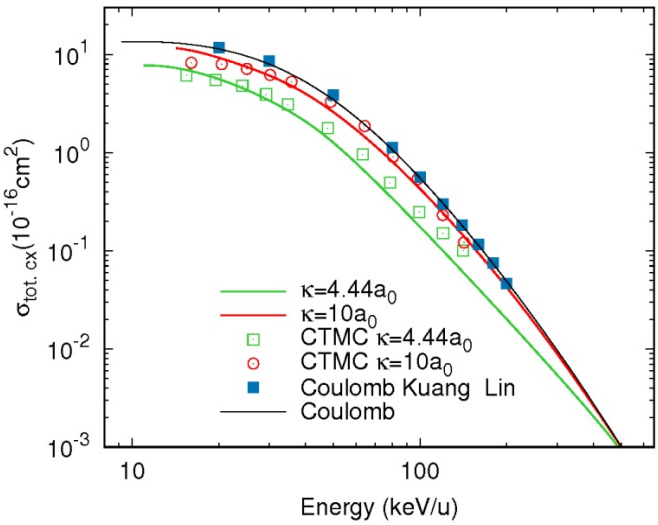

Fig. 7. Total electron capture cross sections for plasmas with screening lengths $\kappa = 4.44a_0$ and $\kappa=10a_0$ and for the plasma-free case. Present results: ful lines; symbols: results from Ref [12] (screened interaction) and Ref. [20] (unscreened Coulomb interaction).

C. IONIZATION

Since in the expansion basis (5) we have included 117 continuum pseudostates centered on the target H, the transitions to these states in the course of the collision would describe the ionization process. The total ionization cross section is given by Eq. (7c), where the summation runs over all continuum pseudostates. As discussed in the Introduction, in the

screened potential (1) for any finite value of the scaled screening length κ_0 the number of bound states is finite. From Table 1 it follows that for a given value κ_0 bound are the nl-states with critical screening lengths satisfying the relation $\kappa_{nl}^c < \kappa_0$, while all the states with $\kappa_{nl}^c > \kappa_0$ lie in the continuum i.e. become continuum pseudostates. Thus, for $\kappa_0=30a_0$ bound in the potential (2) are only the states with $n \leq 4$ (cf. Table 1) and all the $5l$, $6l$ and $7s$ included in our discrete Coulomb basis on H (see Section III) become continuum pseudostates. When calculating the ionization cross section for a given κ_0, the population of the continuum pseudostates, that are generated from entering the discrete states with $\kappa_{nl}^c > \kappa_0$ into the continuum, have also to be included in the sum of Eq. (7c).

In Fig.8 we show the ionization cross sections for plasmas with screening lengths κ = 5, 10, 25, 50a_0 in the energy range ~15- 600keV/u. For the above values of κ the only bound states in the potential (2) are: 1s, (for 5a_0), $n \leq 2$ (for 10a_0), $n \leq 3+4s$ (for 25a_0), and $n \leq 5$ (for 50a_0). In the same figure we also show the cross section for the pure Coulomb interaction. We note that the ionization cross section of Ref. [20] for the pure Coulomb case coincides with the result of our calculations, but is not shown in Fig.8 to preserve the clarity of the figure in the high energy part.

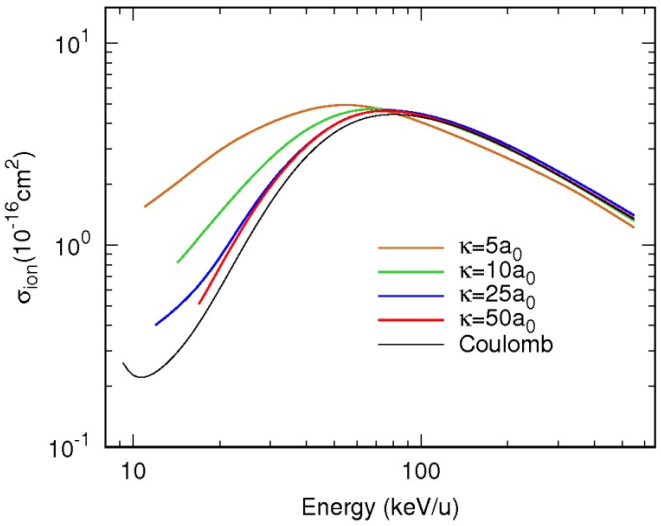

Fig. 8. Ionization cross sections for plasmas with screening lengths κ= 5, 10, 25, 50a_0 and for the pure Coulomb interaction.

In Fig. 8 two different dependences of the ionization cross section on the screening length are observed. For energies above ~70-80keV/u, where the cross section maxima appear, the screened cross sections rapidly tend towards the unscreened cross section when the screening length increases (i.e. they decrease with decreasing κ). In contrast to this, for energies below ~70-80keV/u, the ionization cross section increases with decreasing κ. This increase can be related to the fact that with decreasing κ increasingly more bound states in the expansion basis centered on the target H enter in the continuum. This increases the density of continuum pseudostates and, consequently, the ionization cross section. It is to be noted in Fig. 8 that with decreasing κ also the cross section maximum shifts to lower energies. The relatively weak dependence of the cross section on κ at high energies is result of the fact that the energies of continuum pseudostates, generated by entering of bound states into the continuum when κ decreases, are small and due to the fact that at high collision energies the electron is ejected from the atom to the high-energy continuum states.

V. CONCLUSIONS

In the present work we have studied the excitation, electron capture and ionization processes in collisions of He^{2+} ions with hydrogen atoms in a dense quantum plasma. The interaction between charged particles in such a plasma is represented by the Debye-Hűckel-cosine (DHC) screened potential. The collision dynamics of considered processes is described by the two-center atomic orbital close coupling method with an expansion basis containing 35 bound states centered on the projectile and 57 bound plus 117 continuum pseudostates centered on the target. The investigations of plasma screening effects on the considered processes reveal significant changes in their cross sections with respect to those in the plasma-free case, when the interaction is purely Coulombic. These effects are particularly strong when the screening strong (small screening lengths) and for the smaller collision energies (long collision times). The property of DHC screened potential to support a finite number of bound states for any finite value κ_0 of its screening length (implying that for $\kappa > \kappa_0$ higher states lie in the continuum) has a dramatic effect on the low-energy ionization cross section (dramatic increase with decreasing of κ

and the energy). For the processes taking place within the discrete spectrum (excitation and electron capture, this property of DHC potential limits the collision dynamics to a limited number of bound states, as opposed to the theoretically infinite number of bound states in the case of pure Coulomb potential.

References

[1] P. Debye and E. Hückel, Phys. Z. **24**,185 (1923)

[2] R.K. Janev, S.B. Zhang and J.G. Wang, Matter and Radiation at Extremes **1**, 237 (2016).

[3] P.K. Shukla and B. Eliasson, Phys. Lett. A **372**, 2897 (2008)

[4] A. Ghoshal and Y.K. Ho, J. Phys. B **42**, 175006 (2009)

[5] I. Nasser, M.S. Abdelmonem and A. Abdel-Hady, Phys. Scr. **84**, 045001 (2011)

[6] A. Ghoshal and Y.K. Ho, Phys. Scr. 83, 065301 (2011)

[7] A. Bhattacharya, Z.M. Kamali, A. Ghoshal and K. Ratnavelu, Phys. Plasmas **20**, 083514 (2013)

[8] S. Nayek and A. Ghoshal, Phys. Scr. **85**, 035301 (2012)

[9] N. F. Lai, Y.C. Lin, C.Y. Lin and Y.K. Ho, Chinese J. Phys. **51**, 73 (2013)

[10] C.Y. Lin and Y.K. Ho, Comp. Phys. Commun. **182**, 125 (2011)

[11] L.-Y. Zhang, X. Qi, X.-Y. Zhao, D.-Y. Meng, G.-Q. Xiao, W.-S. Duan and L. Yang, Phys. Plasmas **20**,113301 (2013)

[12] L.-Y. Zhang, X.-Y. Zhao, J.-F. Wan, G.-Q. Xiao, W.-S. Duan, X. Qi and L.Yang, Phys. Plasmas **21**,093302 (2014)

[13] Y.Y. Qi, J.G. Wang and R.K. Janev, Phys. Plasmas **23**, 073302 (2016)

[14] D. Jakimovski, N. Markovska and R.K. Janev, J. Phys. B: At. Mol. Phys. **49**, 205701(2016)

[15] Y.Y. Qi, J.G. Wang and R.K. Janev, Phys. Plasmas **24**, 062110 (2017)

[16] L.D. Landau and E.M. Lifshitz, *Quantum Mechanics: Non-Relativistic Theory* (Pergamon, London, 1958)

[17 W. Fritsch, and C.D. Lin, Phys. Rep. **202**, 1 (1991)

[18] B.H. Bransden and M.R.C. McDowell, *Charge Exchange and the Theory of Ion-Atom Collisions* (Clarendon Press, Oxford, 1992).

[19] C.M. Reeves, J. Chem. Phys. **39**, 1 (1963)

[20] J. Kuang and C.D. Lin, J. Phys. B **30**, 101 (1997)

Прилози, Одд. за тех. науки, МАНУ, XXXVIII, 1–2 (2017) стр, 31–57
Contributions, Sec. Tech. Sci., MANU XXXVIII, 1–2 (2017) pp. 31–57
ISSN 1857–6656
UDC: 539.184.3/.5:59.124-14]:[546.45:546.34

SPIN-RESOLVED STATE-SELECTIVE ELECTRON CAPTURE AND EXCITATION IN BE^{3+}-LI COLLISIONS

L. Liu[1], C. H. Liu[2], D. Jakimovski[3], N. Markovska[4], J. G. Wang[1] and R. K. Janev[4]

[1] Data Center for High Energy Density Physics, Institute of Applied Physics and Computational Mathematics, PO Box 8009-26, Beijing 100088, People's Republic of China
[2] Department of Physics, Southeast University, Nanjing 210094, People's Republic of China
[3] Faculty of Natural Sciences and Mathematics, Sts. Cyril and Methodius University, Skopje, Macedonia
[4] Macedonian Academy of Sciences and Arts, PO Box 428, 1000 Skopje, Macedonia

Abstract: The electron capture in Be^{3+}-Li(2s) collisions is investigated by the quantum-mechanical molecular orbital close-coupling (QMOCC) method and by the two-center atomic orbital close-coupling (TC-AOCC) method in the energy ranges 10^{-4}-1.2keV/u and 0.5-100keV/u, respectively. Spin-resolved total and state-selective cross sections are calculated with large expansion MO and AO basis sets. In the overlapping energy range the results of the two sets of calculations for the total and n=4, 3-shell capture cross sections agree very well for both singlet and triplet channels. Good mutual agreement in this energy range between the two calculations is obtained also for the spin-resolved 4l, 3l cross sections. It is found that the total and n=4 shell singlet and triplet cross sections differ significantly from each other in the energy region below 0.1keV/u, while for the 4l cross sections this difference becomes considerable already at 1keV /u. For the weak n=3 and n=2 capture channels the difference between singlet and triplet cross sections is much smaller. The exci-

tation 2*s*-2*p* cross section for Li in this collision system has also been calculated and no significant difference between the singlet and triplet cross sections was found in the entire energy range considered.

I. INTRODUCTION

Electron capture and excitation processes in multicharged ion - atom collisions have attracted considerable theoretical and experimental attention in the past because of their important role in a wide range of laboratory and astrophysical plasmas [1]. The investigations of collision processes involving Li atom have been motivated both by the cross section data needs for the development of neutral lithium beam spectroscopy diagnostics of edge plasmas in experimental fusion devices [2-4] and by the recently proposed novel concepts for reduction of the excessive thermal loads on divertor plates of tokamak-type fusion reactors by using liquid lithium coatings [5, 6]. The inelastic collision processes of Li atom with plasma ions play a dominant role in both the beam penetration dynamics and the population of radiating levels of Li atoms. On the other hand, beryllium is envisaged as the first wall material in the International Thermonuclear Experimental Reactor [7]. Therefore, the ion-atom collision processes involving these two species are of considerable interest in the current thermonuclear fusion research. In particular, the cross sections of various inelastic processes of Be-ions in all charge states with Li atoms are required for modeling and diagnostics of fusion edge and divertor plasmas.

In the present work we shall study the electron capture and excitation processes in Be^{3+}+Li collisions, for which, to the best of our knowledge, no theoretical or experimental studies have been reported so far. We shall employ the full quantum-mechanical molecular orbital close-coupling (QMOCC) and the two-center atomic orbital close-coupling (TC-AOCC) methods in the 10^{-4}-1.2 keV/u and 0.5 -100keV/u energy ranges, respectively.

The main motivation of the present work is to generate accurate spin-resolved electron capture and excitation cross sections for this collision system in a wide energy range to cover both the modelling and diagnostic needs for such data in the fusion plasma research.

The paper is organized as follows. In the next section, we briefly outline the theoretical methods used in the cross section calculations. In Sec. Ⅲ we present the results of *ab initio* molecular structure calculations, required for the QMOCC cross section calculations, obtained by using the multireference single- and double-excitation configuration interaction (MRDCI) method [8, 9]. In Sec. Ⅳ we present and discuss the results for spin-resolved total and state-selective electron capture and $2s \rightarrow 2p$ excitation cross sections, and in Sec. Ⅴ, we give our conclusions.
Atomic units will be used throughout, unless explicitly indicated otherwise.

II. COMPUTATIONAL METHODS

A. TC-AOCC method

The details of the TC-AOCC method can be found in the literature [10, 11] and here only a brief account is presented. The total electron wave function of the active electron in the TC-AOCC method is expanded in terms of bound atomic orbitals of the two ionic centers (ϕ^A, ϕ^B), multiplied by plane wave electron translational factors $f^{A,B}$,

$$\Psi(\vec{r},t) = \sum_i a_i(t)\phi_i^A(\vec{r},t) f^A(r,t,v) + \sum_j b_j(t)\phi_j^B(\vec{r},t) f^B(r,t,v) \quad (1)$$

where v is the collision velocity.
The atomic states are determined by diagonalizaiton of single-center Hamiltonian over the even-tempered basis [10]

$$\phi_{nlm}(\vec{r}) = \sum_k c_{nk}\chi_{klm}(\vec{r}) \quad (2)$$

Adopting the straight line trajectory approximation for the relative nuclear motion $\vec{R}(t) = \vec{b} + \vec{v}t$ (b is the impact parameter) and inserting the expansion (1) into the time dependent Schrödinger equation $(H - i\frac{\partial}{\partial t})\Psi = 0$, where $H = -\frac{1}{2}\nabla_r^2 + V_A(\vec{r}_A) + V_B(\vec{r}_B)$ and $V_{A,B}(\vec{r}_{A,B})$ are the

active electron interactions with the projectile Be^{3+} and target core Li^{+}, respectively, one obtains the first-order coupled differential equations for the amplitudes $a_i(t)$ and $b_j(t)$

$$\begin{aligned} i(\dot{A} + S\dot{B}) &= HA + KB \\ i(\dot{B} + S^{\dagger}\dot{A}) &= \bar{K}A + \bar{H}B \end{aligned} \tag{3}$$

where A and B are the vectors of amplitudes a_i*(i*=1, 2, ..., N_A*)* and b_j *(j*=1, 2, ..., N_B*)*, respectively. *S* is the overlap matrix ($S^{\dagger}$ is its transposed form), *H* and $\bar{H}$ are direct coupling matrices, and *K* and $\bar{K}$ are the electron exchange matrices.

The interactions $V_{A,B}(r_{A,B})$ of the active electron with the ionic cores B^{3+} and Li^{+} we shall represent by model potentials. Since Be^{3+} ion has a 1*s* bound electron, the capture states Be^{2+}(1*snl*) form two series of states, differing by their total spin (singlet or triplet) and binding energies. The electron-ionic core interaction in such He-like systems has been studied by Bottcher [12] and using his procedure we have obtained the numerical values oh the singlet and triplet potentials for the (Be^{3+}+e) system and then fitted to the analytic forms

$$V_{A,singlet}(r) = -\frac{3.0}{r} - \frac{0.74146}{r}e^{-11.0r} - 7.0e^{-11.0r} \tag{4a}$$

$$V_{A,triplet}(r) = -\frac{3.0}{r} - \frac{1.2}{r}e^{-6.2r} - 4.2e^{-6.2r} \tag{4b}$$

Except for the ground state, the calculated energies of Be^{2+}(1*snl*) states with these potentials agree with the NIST data [13] to within 1.7% for the singlet states and 1.9% for the triplet states. For the potential $V_B(r)$ we have used the model potential from Ref. [14]

$$V_{B,Li}(r) = -\frac{1}{r} - \frac{2}{r}e^{-3.310r} - 3.310e^{-3.310r} \tag{5}$$

The coupled equations (3) are solved separately for the singlet and triplet potentials $V_A(r)$ subject to the initial conditions

$$a_i(-\infty) = 0, b_j(-\infty) = \delta_{j1} \tag{6}$$

and the cross sections for 1→*i* electron capture and 1→*j* excitation transitions within each spin multiplicity are obtained by integration of corresponding probabilities over the impact parameter *b*

$$\sigma_{cx,i}^{s,t} = 2\pi \int_0^\infty \left|a_i(+\infty)\right|^2 b db \tag{7}$$

$$\sigma_{ex,j}^{s,t} = 2\pi \int_0^\infty \left|b_j(+\infty)\right|^2 b db \tag{8}$$

The spin-averaged cross section for the *i*-th electron capture channel is obtained as $\sigma_{cx,i} = \frac{1}{4}\sigma_{cx,i}^{s} + \frac{3}{4}\sigma_{cx,i}^{t}$ and similarly for $\sigma_{ex,j}$.

B. QMOCC method

Details of the QMOCC method for ion-atom collisions can be found elsewhere [15, 16] and only its basic elements of the method are outlined here. The active electron wave function now is expanded over adiabatic states of $BeLi^{2+}$ molecular ion and its replacement in the time-dependent Schrödinger equation result in a system of coupled second-order differential equations. The system of coupled equations is normally solved by using the log-derivative method of Johnson [17]. In the adiabatic representation of molecular states, the transitions between the states are driven by radial and rotational (A^r and A^θ) couplings of the vector potential $\vec{A}(\vec{R})$, where *R* is the internuclear distance vector. Since in the adiabatic representation the matrix elements of A^r at internuclear distances R where two molecular states of the same overall symmetry have quasi-degenerate energies become extremely large over a narrow ΔR region, it is numerically convenient to perform a unitary transformation of the adiabatic expansion basis into a diabatic one [18]. The electron translation effects in the electron capture process can be accounted for by transforming the radial and rotational coupling matrix elements between the states χ_α and χ_β into [19]

$$\begin{matrix} \left\langle \chi_\alpha \left| \partial / \partial R - (\varepsilon_\alpha - \varepsilon_\beta) z^2 / 2\,\mathrm{R} \right| \chi_\beta \right\rangle \\ \left\langle \chi_\alpha \left| iL_y + (\varepsilon_\alpha + \varepsilon_\beta) zx \right| \chi_\beta \right\rangle \end{matrix} \tag{9}$$

where ε_α and ε_β are the energies of the two states, and z^2 and zx are the components of the quadrupole moment tensor. The modification is similar in form to that resulting from the application of the common translation factor method [20].

With the diabatic potentials and couplings, the coupled second order differential equations are solved and their solutions matched to the plane-wave boundary conditions at a large internuclear distance $R_{\max}$ to obtain the K matrix. Then the scattering matrix S is given

$$S_J = [I + iK_J]^{-1}[I - iK_J] \tag{10}$$

where I is the identity matrix and J is the total angular momentum quantum number. Finally, the charge transfer cross section for transition from a state α to a state β is expressed in terms of scattering matrix elements

$$\sigma_{\alpha\to\beta} = \frac{\pi}{k_\alpha^2} \sum_J (2J+1) \mid \delta_{\alpha\beta} - S_{\alpha\beta}^J \mid^2 \tag{11}$$

where k_α is the initial momentum of the center-of-mass motion.

The QMOCC coupled equations for the singlet and triplet states are solved separately and the spin-averaged cross section for the channel $\alpha \to \beta$ is a weighted sum of the corresponding singlet and triplet cross sections.

III. MOLECULAR STRUCTURE CALCULATIONS

The MRDCI package was employed to calculate the potential energy curves, the radial and rotational coupling matrix elements. The correlation-consistent, polarization valence, triple-zeta (cc-pVTZ) type basis set [21] with a diffuse (*2s2p2d2f*) basis was employed for Be atom. For Li

atom, an effective core potential (ECP) with the ECP-adapted (*4s4p*) Gaussian basis set [22] was used.

We have calculated the lowest twenty-three singlet states and twenty-two triplet states, involving twelve $^1\Sigma$, seven $^1\Pi$, three $^1\Delta$, one $^1\Phi$ states and eleven $^3\Sigma$, seven $^3\Pi$, three $^3\Delta$, one $^3\Phi$ states of $BeLi^{3+}$ molecule, respectively. Figs.1(a) and 1(b) show the adiabatic potential energy curves of $BeLi^{3+}$ for the singlet and triplet states, respectively, in the internuclear distances of R=0-40a_0. Fig.1 shows that both in the singlet and triplet case the energy curve of the entrance Be^{3+}-Li(2s) state intersects (in a diabatic picture) the energies of the $Be^{2+}(n=4)+Li^+$ states and only in the region R<10a_0 it becomes close to the energy curves of the n=3 states. This indicates that the n=4 states will be the dominant electron capture channels in Be^{3+}+Li(2s) collisions. Fig.2 displays the expanded form of the adiabatic potential curves of the initial $11^1\Sigma$ and $10\ ^3\Sigma$ states together with the singlet and triplet states that asymptotically correlate to the $Be^{2+}(n=4)+Li^+$ atomic states. From these figures it can be seen that the energies of initial $11^1\Sigma$ and $10\ ^3\Sigma$ states undergo avoided crossings with the energies of $Be^{2+}(1s4l)+Li^+$ states in the R~18-29a_0 region. It should be noted that the $Be^{2+}(1s3p)$ and $Be^{2+}(1s3d)$ states as well as the $Be^{2+}(1s4p)$, $Be^{2+}(1s4d)$ and $Be^{2+}(1s4f)$ states in singlet manifold are inverted, while in the triplet manifold all states are in normal order of decreasing the binding energy with increasing the angular quantum number l within the n- shell. This would lead to significant differences in the magnitudes and energy dependences of singlet and triplet capture cross sections at low energies.

In Table 1 we show the molecular states included in the MRDCI calculations for $BeLi^{3+}$ together with the atomic states to which they converge in the asymptotic region of internuclear distances R and their asymptotic energies, obtained by extrapolation of calculated energies at R = 100a_0 to infinity by Coulomb and zero interactions for the electron capture and entrance channels, respectively. The calculated energies are compared with those from the NIST tables [13].

Table 1.

Asymptotic separated-atom energies of $BeLi^{3+}$ molecule.

Molecular state	Asymptotic atomic state	Energy (eV)		
		Expt. [13]	Theor.	error
$1^3\Sigma^+$	$Be^{2+}(1s2s)[^3S]+Li^+$	-29.913	-29.676	0.237
$2^1\Sigma^+$	$Be^{2+}(1s2s)[^1S]+Li^+$	-26.854	-26.724	0.13
$2^3\Sigma$, $1^3\Pi$	$Be^{2+}(1s2p)[^3P]+Li^+$	-26.583	-26.363	0.22
$3^1\Sigma$, $1^1\Pi$	$Be^{2+}(1s2p)[^1P]+Li^+$	-24.836	-24.715	0.121
$3^3\Sigma^+$	$Be^{2+}(1s3s)[^3S]+Li^+$	-9.495	-9.363	0.132
$4^1\Sigma^+$	$Be^{2+}(1s3s)[^1S]+Li^+$	-8.687	-8.634	0.053
$4^3\Sigma$, $2^3\Pi$	$Be^{2+}(1s3p)[^3P]+Li^+$	-8.613	-8.591	0.022
$5^3\Sigma$, $3^3\Pi$, $1^3\Delta$	$Be^{2+}(1s3d)[^3D]+Li^+$	-8.231	-8.155	0.076
$5^1\Sigma$, $2^1\Pi$, $1^1\Delta$	$Be^{2+}(1s3d)[^1D]+Li^+$	-8.221	-8.150	0.071
$6^1\Sigma$, $3^1\Pi$	$Be^{2+}(1s3p)[^1P]+Li^+$	-8.106	-8.052	0.054
$6^3\Sigma$	$Be^{2+}(1s4s)[^3S]+Li^+$	-2.786	-2.579	0.207
$7^1\Sigma$	$Be^{2+}(1s4s)[^1S]+Li^+$	-2.450	-2.347	0.103
$7^3\Sigma$, $4^3\Pi$	$Be^{2+}(1s4p)[^3P]+Li^+$	-2.429	-2.327	0.102
$8^3\Sigma$, $5^3\Pi$, $2^3\Delta$	$Be^{2+}(1s4d)[^3D]+Li^+$	-2.271	-2.151	0.12
$8^1\Sigma$, $4^1\Pi$, $2^1\Delta$	$Be^{2+}(1s4d)[^1D]+Li^+$	-2.266	-2.148	0.108
$9^1\Sigma$, $5^1\Pi$, $3^1\Delta$	$Be^{2+}(1s4f)[^1F]+Li^+$	-2.263	-2.138	0.125
$9^3\Sigma$, $6^3\Pi$, $3^3\Delta$	$Be^{2+}(1s4f)[^3F]+Li^+$	-2.263	-2.138	0.125
$10^1\Sigma$, $6^1\Pi$	$Be^{2+}(1s4p)[^1P]+Li^+$	-2.224	-2.084	0.140
$11^1\Sigma$, $10^3\Sigma$	$Be^{3+}(1s)+Li(2s)$	0	0	0
$12^1\Sigma$, $11^3\Sigma$, $7^{1,3}\Pi$	$Be^{3+}(1s)+Li(2p)$	1.848	1.848	0

Figs. 3 and 4 display the radial and rotational coupling matrix elements between the states shown in Fig.2, respectively. There exit series of strong radial couplings between the entrance channels with the Σ states of the n=4 series in the R~18-29a_0 region. These couplings will effectively populate the $Be^{2+}(1s4l)+Li^{+}$ capture states at large internuclear distances in the approaching stage of the collision. The rotational couplings will mainly redistribute the capture flux among the states within the same nl-subshell in the receding stage of the collision.

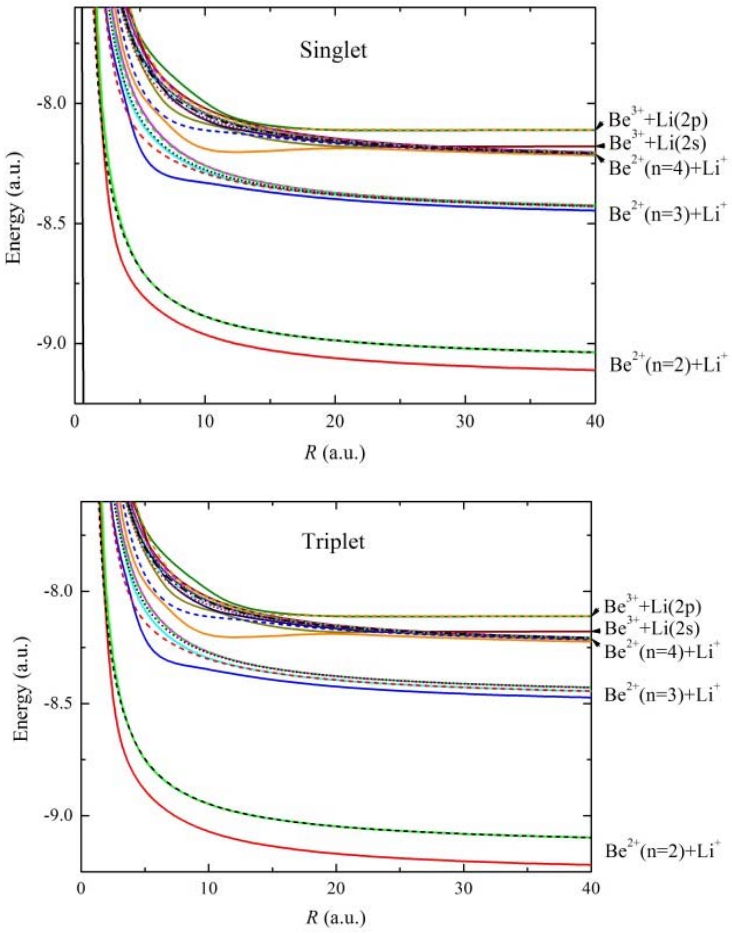

Fig. 1. (Color online) Adiabatic energies of $BeLi^{3+}$ molecular ion. The solid, dashed, dotted and dash-dotted lines represent the Σ, Π, Δ and Φ states, respectively. (a)Singlet states; (b)triplet states.

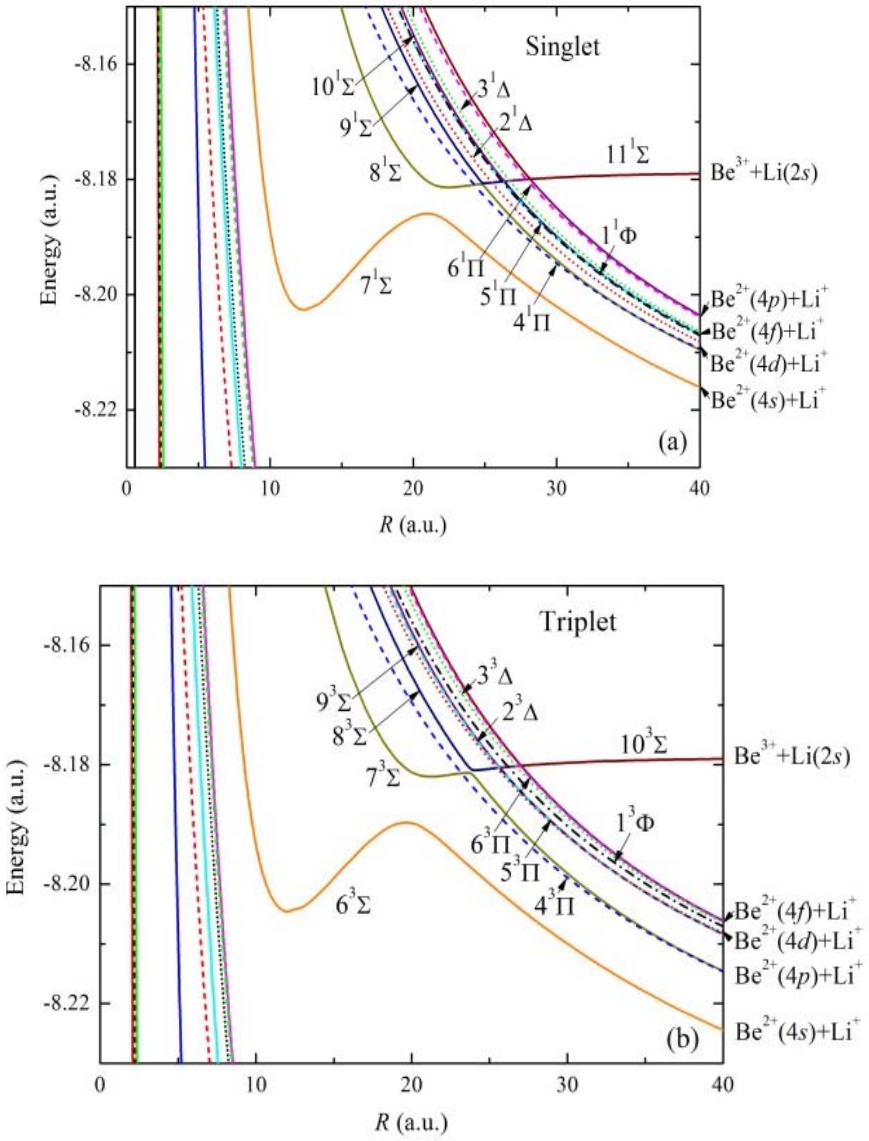

Fig. 2. (Color online) Enlarged view of adiabatic energies of $BeLi^{3+}$. (a) Singlet states; (b) triplet states.

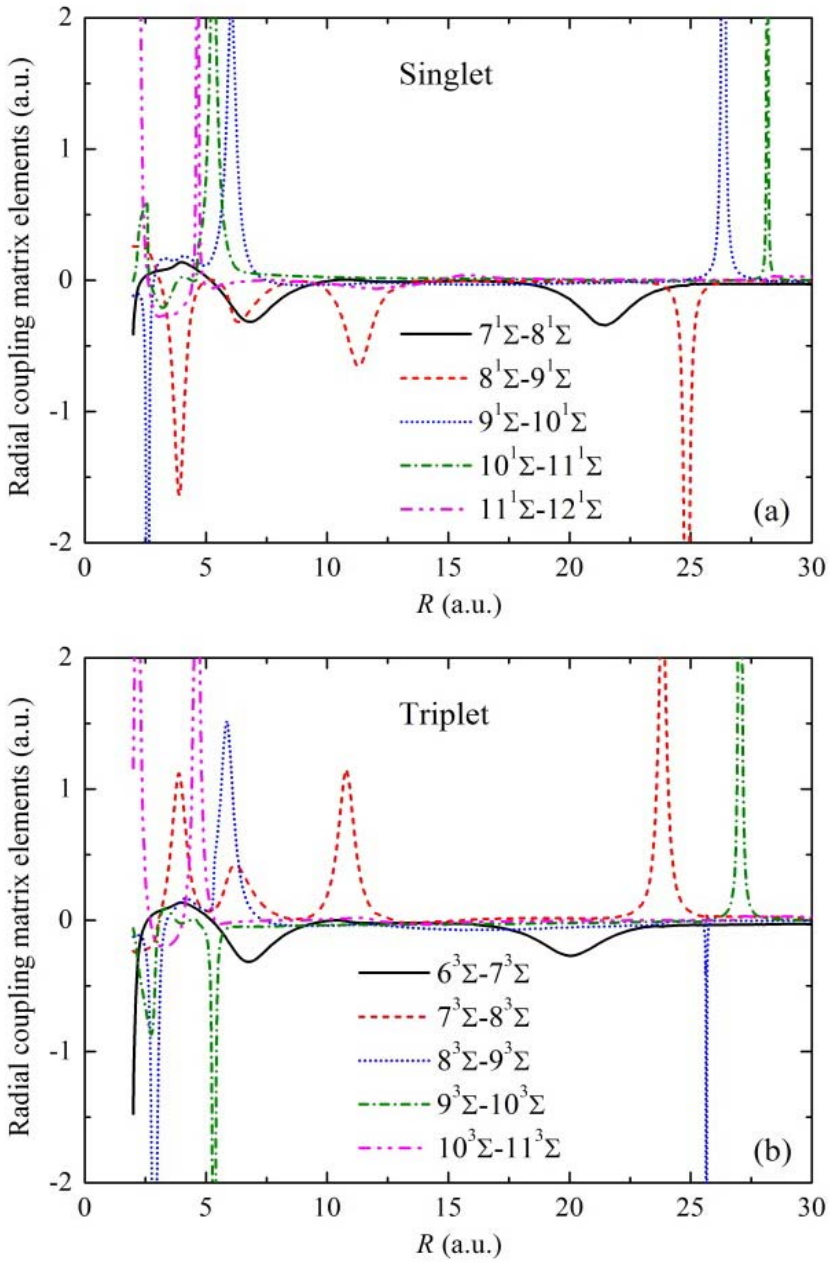

Fig. 3. (Color online) Radial coupling matrix elements. (a) Singlet states; (b) triplet states.

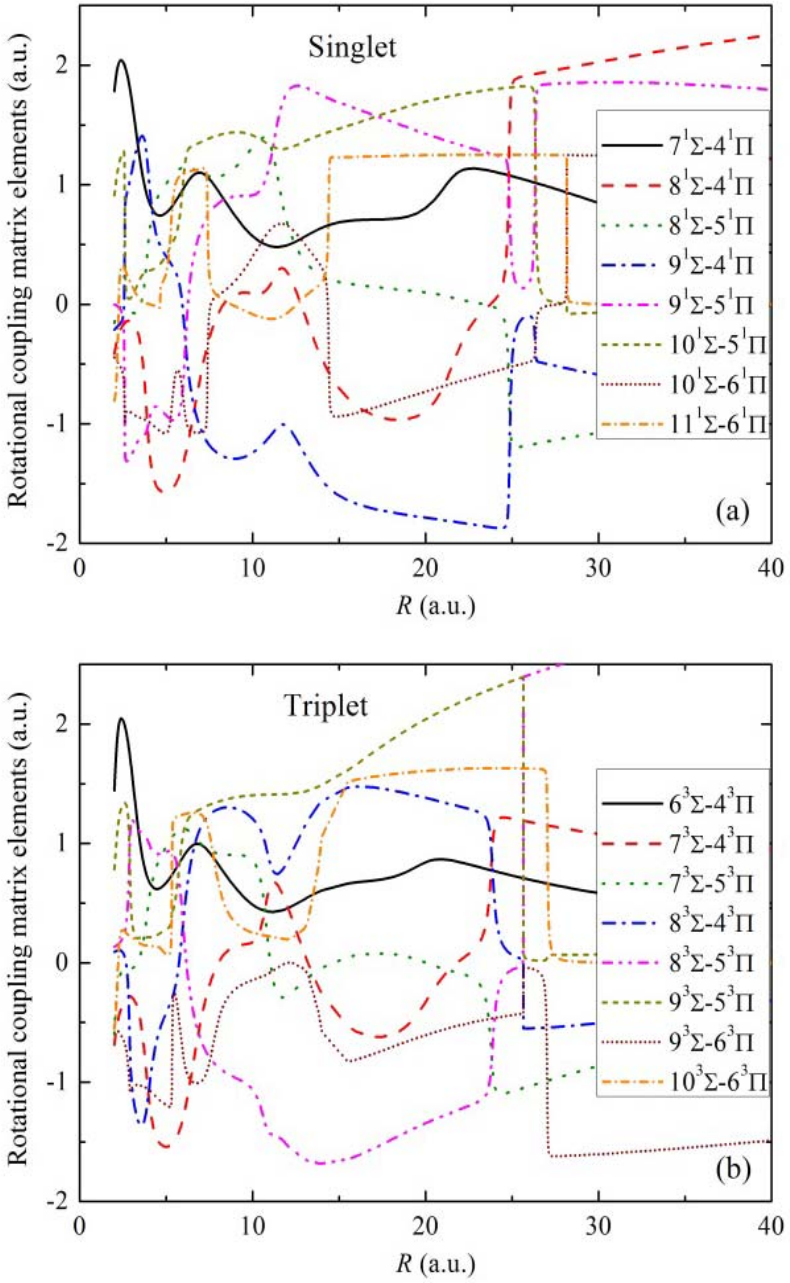

Fig. 4. (Color online) Rotational coupling matrix elements. (a) Singlet states; (b) triplet states.

IV. RESULTS AND DISCUSSION

A. Electron capture cross sections

The electron capture cross sections of Be^{3+}-Li(2s) collision were calculated by the QMOCC and TC-AOCC methods in the energy range of 10^{-4}-1.2keV/u and 0.5-100keV/u, respectively. In the QMOCC calculations, we have included all 23 singlet and 22 triplet molecular states in the corresponding expansion basis at energies above 0.5 eV/u and at lower energies, we discarded the Be^{3+}-Li(2p) states. In the TC-AOCC calculations, for energies above 3keV/u the basis set centered on Li includes all $n \leq 4$ bound states, while the basis centered on Be^{3+} ion included all $n \leq 10$ (l=0-5) bound states plus 42 positive-energy pseudostates. For energies below 3keV/u, the basis set centered on Li was kept the same, but the one centered on Be^{3+} was reduced to include only the bound states with $n \leq 9$ (l=0-5) since in this energy region capture to the projectile continuum is negligible.

Spin-averaged cross sections

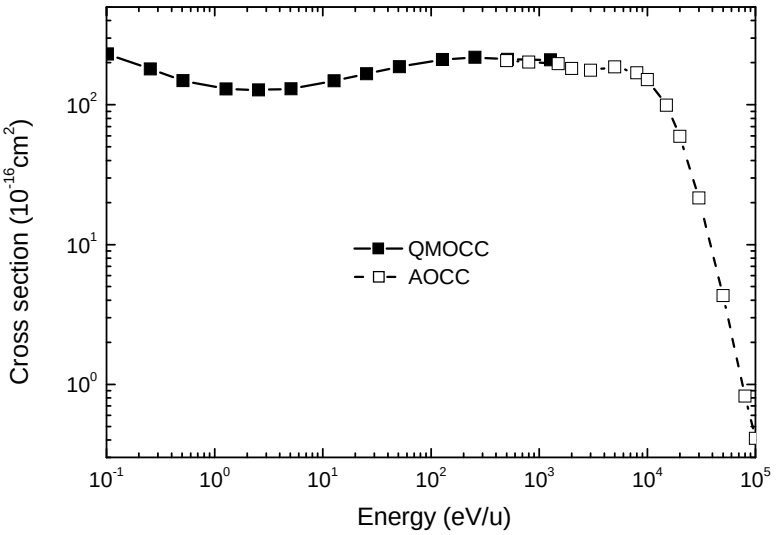

Fig. 5. Total electron capture cross section in Be^{3+}-Li(2s) collisions as a function of collision energy.

The total spin-averaged QMOCC and TC-AOCC electron capture cross sections for the Be^{3+}-Li collision are displayed in Fig. 5 in the energy range 10^{-4}-100keV/u. The two cross sections are in excellent agreement with each other in the overlapping energy range. The total cross section exhibits a broad maximum in the 0.1-2.0keV/u energy range, a broad valley around 2eV/u, a slow increase ~1eV/u and a sharp decrease for energies above 10keV/u. We note that when the TC-AOCC calculations are extended down to 0.1keV/u the total spin-averaged cross section continues to agree very well with the QMOCC cross section, but when the QMOCC calculations are extended above 1.2keV/u the QMOCC cross section starts rapidly to increase above the TC-AOCC cross section.

Spin-resolved cross sections

The total QMOCC and TC-AOCC cross sections for electron capture to the singlet and triplet states of Be^{2+} ion are shown in Fig. 6. In the overlapping energy range the results of QMOCC and TC-AOCC calculations for both spin manifolds agree very well. The most important information contained in this figure is, however, that the total singlet and triplet cross sections in the energy region below ~0.1keV/u are significantly different from each other and have different energy behavior. In contrast, in the energy range ~0.25-30keV/u the two cross sections almost coincide and only for energies above 30keV/u they start to differ appreciably. Generally speaking, the difference in the magnitude of singlet and triplet capture cross sections at low collision energies is a consequence of the sensitivity of the capture process at these energies to the binding energies of capture states (the binding energies of singlet states in an *nl*-subshell of Be^{2+} are always smaller than those for the triplet states) and to the couplings operating between the states within the same spin manifold (cf. Figs 3 and 4). With increasing the collision energy above 0.25keV/u the role of the small energy difference between the spin states within the same *nl*-subshell becomes less important in the capture dynamics, while the role of momentum transfer increases [11], producing the difference between the singlet and triplet cross sections at energies above ~30keV/u. The spin dependence of capture cross sections obviously appears in all two-electron collision systems at low collision energies. The TC-AOCC calculations for the He^{+}+Li collision system [23, 24], in which the singlet-triplet splitting of He(1*s*2*l*) states is very large, have shown a

drastic difference between the singlet and triplet capture cross sections in the energy region below 1keV/u. Spin-resolved total and *n*- and *nl*-selective electron capture cross section calculations have been performed also for the C^{5+} +H collision system by the QMOCC and TC-AOCC methods in [25] and by the TC-AOCC method (with a larger expansion basis) in [26].

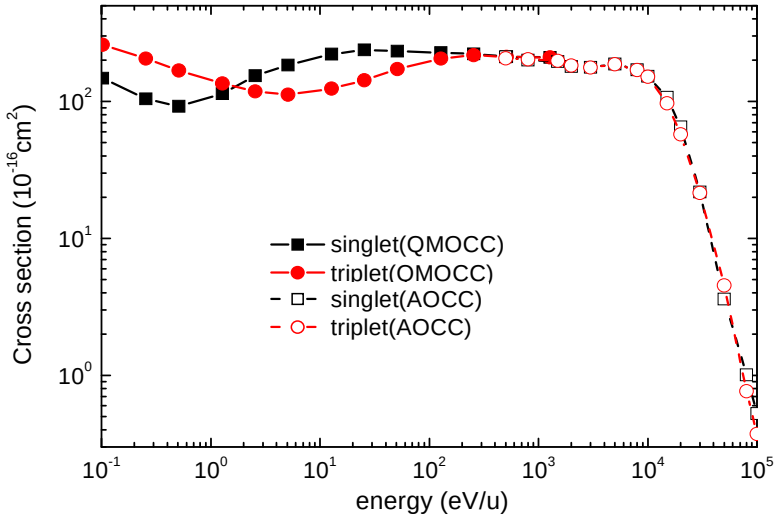

Fig. 6. (Color online) Total cross sections for electron capture to the singlet and triplet states of Be^{2+} ion.

An insight in the electron capture dynamics leading to the differences between the total singlet and triplet capture cross sections observed in Fig.6 can be obtained by analyzing the spin-resolved cross sections for capture to the 1*s*4*l* states of Be^{2+}, which are the dominant capture channels in this collision system in the entire energy range considered. These cross sections are shown in the panels (a) and (b) of Fig. 7, for the singlet and triplet manifolds, respectively. Smooth connection of QMOCC and TC-AOCC results in the overlapping energy range is observed only for the capture to 4*s,* 4*d,* 4*f* singlet and 4*s,* 4*p* triplet states. One reason for the mismatch of the other cross sections is the fact that both methods in this energy range are at the limit of their applicability. Another reason could be the fact that in the molecular basis in the QMOCC calculations

does not include the states converging to the $Be^{2+}(n \geq 5)$ and $Li(n \geq 3)$ asymptotic states that are included in the AO expansion basis. This might particularly affect the 4*p* singlet and 4*f* triplet results as these are the states energetically closest to the *n*=5 groups of singlet and triplet states.

The capture dynamics of the singlet and triplet 4*l* is dominated by the series of radial couplings $11^1\Sigma$ - $10^1\Sigma$ - $9^1\Sigma$ - $8^1\Sigma$ - $7^1\Sigma$ and $10^3\Sigma$ - $9^3\Sigma$ - $8^3\Sigma$ - $7^3\Sigma$ - $6^3\Sigma$ states, respectively, in the range of internuclear distances ~$18a_0$- $29a_0$, where $11^1\Sigma$ and $10^3\Sigma$ are the initial states. The states $7^1\Sigma$, $8^1\Sigma$, $9^1\Sigma$ and $10^1\Sigma$ asymptotically converge to the 4s, $4d_0$, $4f_0$ and $4p_0$ states of Be^{2+} ion, respectively, while the states $6^3\Sigma$, $7^3\Sigma$, $8^3\Sigma$ and $9^3\Sigma$ asymptotically converge to the 4s, $4p_0$, $4d_0$ and $4f_0$ states of Be^{2+}. In the approaching stage of the collision the Σ - Σ couplings in the region R ~$18a_0$- $29a_0$ populate the *m*=0 substates of 4*l* states, while the m > 0 substates of 4*l* states are populated by the rotational Σ- Π, Π-Δ and Δ-Φ transitions in the receding stage of the collision. It should be noted that in Fig.3 that the $11^1\Sigma$ - $10^1\Sigma$ - $9^1\Sigma$ - $8^1\Sigma$ and $10^3\Sigma$ - $9^3\Sigma$ - $8^3\Sigma$ - $7^3\Sigma$ couplings (and the corresponding avoided crossings in Fig.2) are very narrow and at higher energies they are not effective (the avoided crossings are passed "diabatically"). The only effective couplings at such energies are broadly distributed $7^1\Sigma$ - $8^1\Sigma$ and $6^3\Sigma$ - $7^3\Sigma$ couplings at R~ $21.5a_0$ and R~ $20a_0$, respectively, (corresponding to the large avoided crossings in Fig. 2 at the same internuclear distances). These couplings lead to the dominance of the 4*s* singlet and triplet cross sections in Figs. 7a and 7b in the energy ranges ~1-200eV/u and ~20-1000eV/u, respectively. Note that in the regions of their maxima the 4*s* singlet cross section is somewhat larger than the triplet 4*s* cross section, reflecting the somewhat larger magnitude of the $7^1\Sigma$ - $8^1\Sigma$ coupling with respect to the $6^3\Sigma$ - $7^3\Sigma$ coupling (and the smaller energy gap between the $7^1\Sigma$ and $8^1\Sigma$ states with respect to that between $6^3\Sigma$ and $7^3\Sigma$ states; cf. Figs. 3 and 2).

For energies below ~1eV/u and ~10eV/u, due to the larger collision time, the strong $8^1\Sigma$-$9^1\Sigma$, $9^1\Sigma$-$10^1\Sigma$, $10^1\Sigma$-$11^1\Sigma$ and $7^3\Sigma$- $8^3\Sigma$, $8^3\Sigma$- $9^3\Sigma$, $9^3\Sigma$-$10^3\Sigma$ couplings become more effective than the $7^1\Sigma$ - $8^1\Sigma$ and $6^3\Sigma$ - $7^3\Sigma$ couplings leading to 4*p*, 4*d* and 4*f* singlet and triplet cross sections larger

than the corresponding 4*s* ones. We note that to the population of 4p, 4d and 4f singlet and triplet exit channels contribute also the Σ-Π, Π-Δ and Δ-Φ rotational couplings at the relatively small internuclear distances and their cross sections are not determined dominantly by the radial coupling in the R ~ $18a_0$-$29a_0$ range of internuclear distances, like in the case of 4*s* cross sections. Besides, the number of molecular channels contributing to 4*l* states with $l > 0$ increases with increasing l (see Table 1). All these elements of capture dynamics affect the magnitude and energy behavior of the 4*l* ($l > 0$) cross sections different within a given spin manifold and even more so the difference between the 4*l* singlet and triplet cross sections, as exemplified in the panels (a) and (b) of Fig.7.

In the energy region above ~2keV/u the relative magnitudes of 4*l* cross sections of both singlet and triplet manifolds increase with increasing l until E~30keV/u, after which the cross sections with $l > 0$ become close to each other due to the closeness of the binding energies of these capture states.

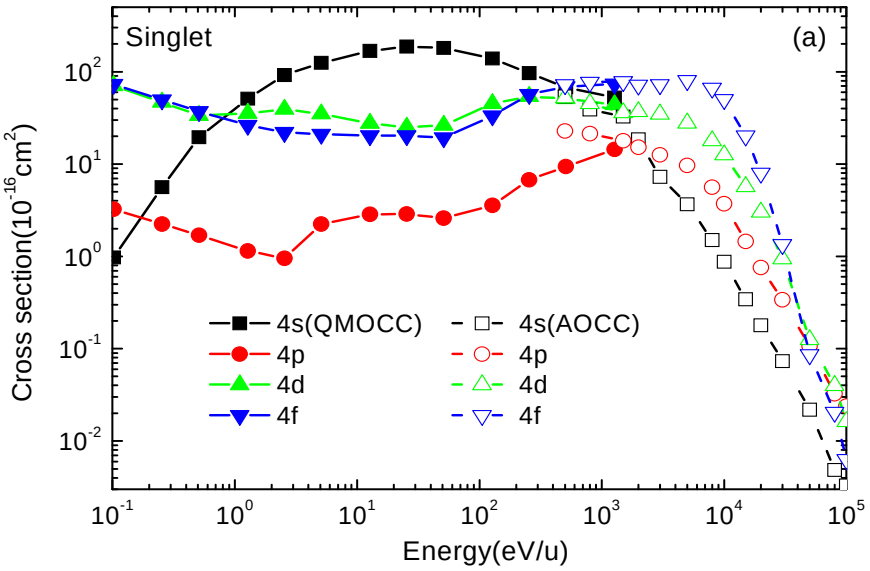

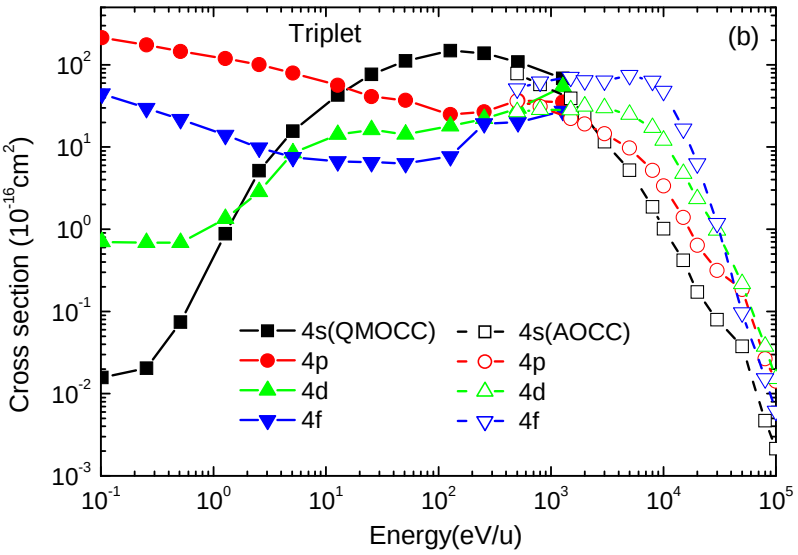

Fig. 7. (Color online) Cross sections for electron capture to 4*l* singlet (panel (a)) and triplet (panel (b)) states of Be^{2+} ion.

In Fig. 8 we show the spin-resolve cross sections for electron capture to the n=4 shell of Be^{2+} ion. In the energy region below ~ 10keV/u the singlet and triplet n=4-shell cross sections are almost identical with the total singlet and triplet cross section in Fig. 6. Only for energies above ~ 20keV/u the spin- resolved cross sections become larger than those for the n=4 shell primarily due to the contribution of n = 3 shell cross sections (see Fig. 10 below). In this energy region the contribution from $n \geq 5$ states to the total singlet and triplet cross sections is about 10%.

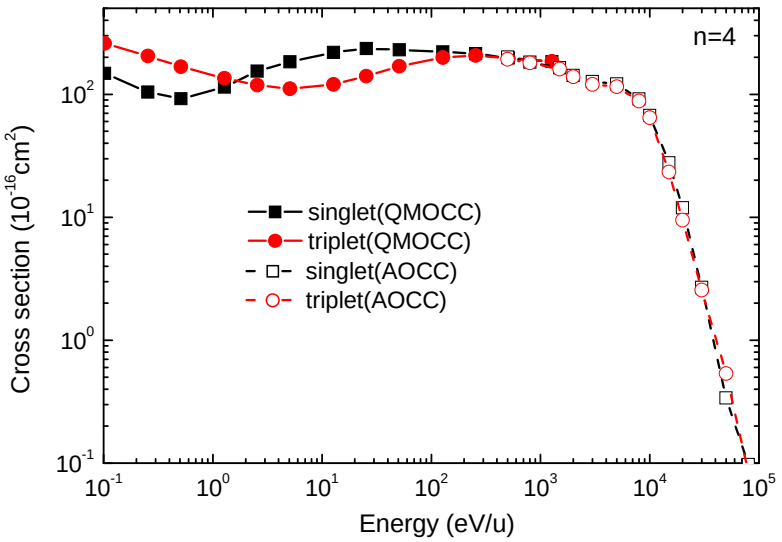

Fig. 8. (Color online) Cross sections for electron capture to the n=4 shell of singlet and triplet states of Be^{2+} ion.

The spin-resolved cross sections for capture to the 3*l* singlet and triplet states of Be^{2+} are shown in Fig.9. The magnitude of these cross sections in the region of their maxima are more than an order smaller than those for capture to corresponding 4*l* states (cf. Figs. 7) and for lower energies this difference increases even more. The mismatch of QMOCC and TC-AOCC results in the overlapping energy range is much larger than in the case of 4*l* states due to the fact that in this energy range both methods are at the limit of their applicability and their uncertainty at this limit is always more pronounced for the weak reaction channels. It is to be noted that the 3*p* and 3*d* cross sections show a steady decrease with decreasing the energy in both the singlet and triplet case, in contrast to their 4*l* counterparts which start to increase below certain value of the collision energy. The large differences in the magnitude and energy behavior between the 3*l* and 4*l* spin-resolved cross sections at low energies is evidence of the different collision dynamics in the population of 3*l* and 4*l* exit channels. Indeed, as Fig.1 indicates, there are no long-distant radial couplings (manifested by avoided crossings) of the initial $11^1\Sigma$ and $10^3\Sigma$ states with the group of molecular states converging to $Be^{2+}(1s3l)$ atomic

states. Only for internuclear distances smaller than R~5a_0 the energies of initial $11^1\Sigma$ and $10^3\Sigma$ states become close to, respectively, the energies of $6^1\Sigma$ and $5^3\Sigma$ states, providing conditions for Demkov-type nonadiabatic couplings. The $6^1\Sigma$ and $5^3\Sigma$ molecular states asymptotically converge to the $3p_0$ singlet and $3d_0$ triplet atomic states of Be^{2+}. The singlet $3d_0$ and triplet $3p_0$ are populated by the $6^1\Sigma$-$5^1\Sigma$ and $5^3\Sigma$-$4^3\Sigma$ Demkov-type couplings, respectively, while the singlet and triplet 3*s* states are populated through the series $6^1\Sigma$-$5^1\Sigma$-$4^1\Sigma$ and $5^3\Sigma$-$4^3\Sigma$-$3^3\Sigma$ of successive couplings, respectively. The rotational Σ-Π, Π-Δ couplings populate the m >0 components of 3*l* states in the receding stage of the collision. Fig.9 shows the direct couplings of the $6^1\Sigma$ and $5^3\Sigma$ states with the entrance $11^1\Sigma$ and $10^3\Sigma$ channels provide the dominance of the 3*p* and 3*d* cross sections within the singlet and triplet 3*l* manifolds in the energy region below ~ 0.5keV/u. The smallest values of the 3s cross sections in both 3*l* manifolds of states are due the involvement of multiple intermediary couplings at each of which the outgoing capture flux is reduced.

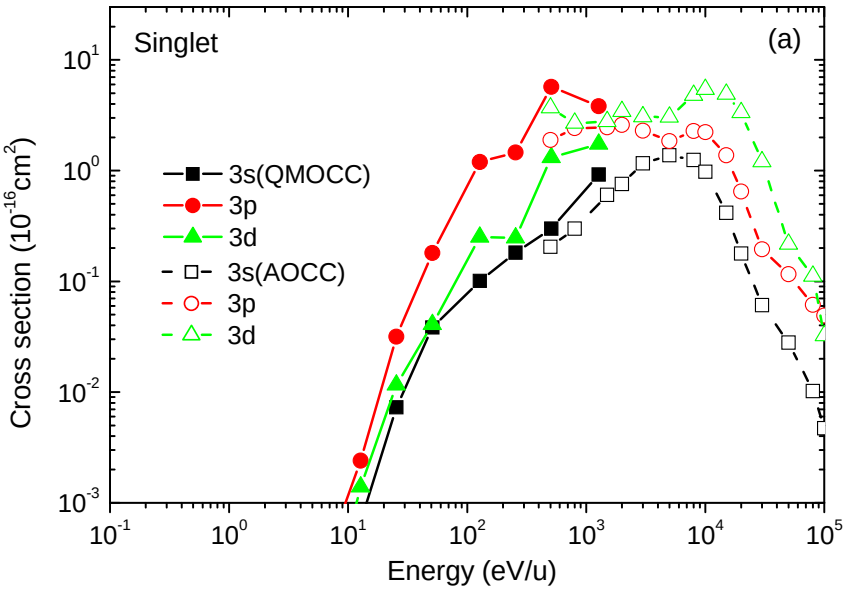

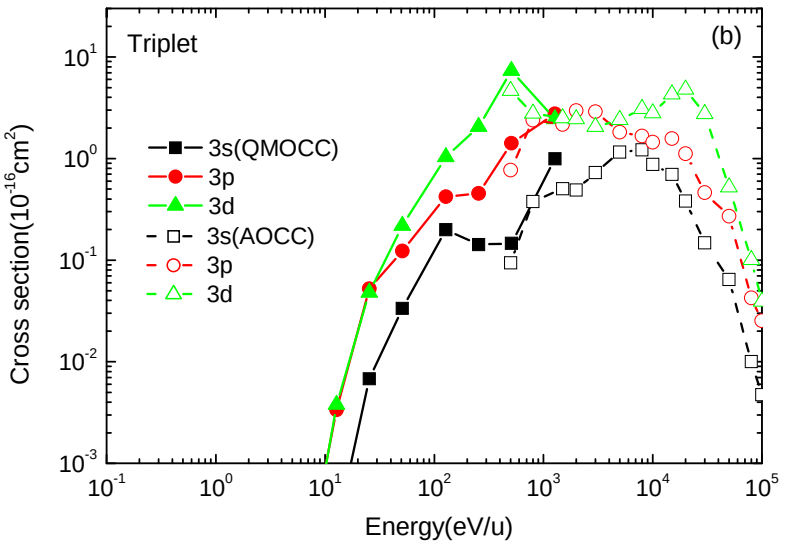

Fig. 9. (Color online) Cross sections for electron capture to 3*l* singlet (panel (a)) and triplet (panel (b)) states of Be^{2+} ion.

The spin-resolved total cross sections for capture to the singlet and triplet manifolds of n=3 shell of Be^{2+} ion are shown in Fig. 10. As in the case of spin-resolved n=4 shell cross sections, the QMOCC and TC-AOCC results in the overlapping energy range agree much better than is the case for the spin-resolved 3*l* cross sections. However, in contrast to the n=4 shell, for which the total singlet and triplet shell cross sections significantly differ from each other in the energy region below ~0.1keV/u, in the present case the singlet and triplet n=3 cross sections are close to each other in the entire energy range investigated.

We have also calculated the spin-resolved QMOCC and TC-AOCC cross sections for capture to 1*s*2*l* states of Be^{2+} ion. These cross sections are an order of magnitude smaller than the corresponding 3*l* cross sections in Fig. 9. In the molecular picture of collision dynamics this is because the energetically deeply lying 2*l* states are populated through couplings with the weakly populated 3*s* states in the receding stage of the collision. Namely, the $2p_0$ single and triplet states are populated through the $4\,^1\Sigma$-

$3^1\Sigma$ and $3^3\Sigma$-$2^3\Sigma$ Demkov-type couplings and the 2s singlet and triplet states through the $3^1\Sigma$-$2^1\Sigma$ and $2^3\Sigma$-$1^3\Sigma$. The $2p_1$ singlet states are populated through the $3^1\Sigma$-$2^1\Pi$ and $2^3\Sigma$-$1^3\Pi$ rotational couplings. In the atomic state picture of collision dynamics the small values of $2l$ capture cross sections results from the large energy differences between the initial states and n=3 group of states and between the n=3 and n=2 groups of states causing weak interstate couplings. The singlet and triplet n=2 shell capture cross sections are shown in Fig. 11.

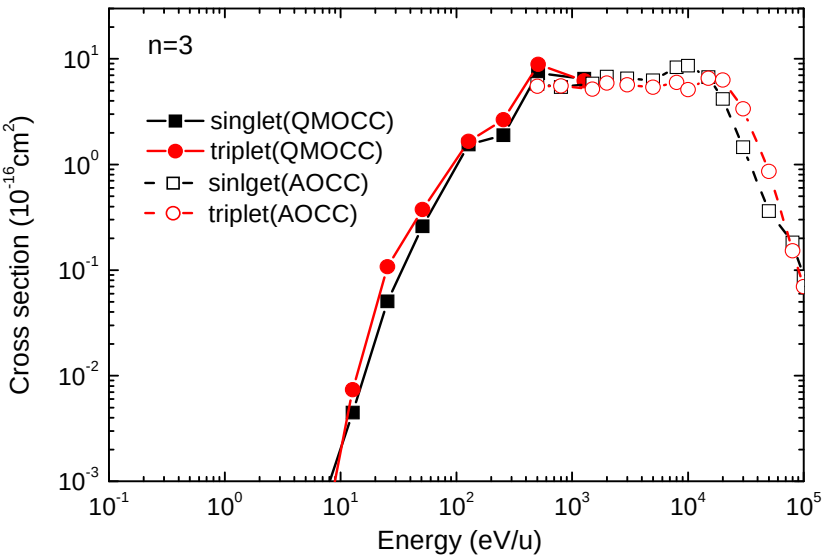

Fig. 10. (Color online) Cross sections for the electron capture to Be^{2+}(n=3) shell of the singlet and triplet states in Be^{3+}-Li collisions.

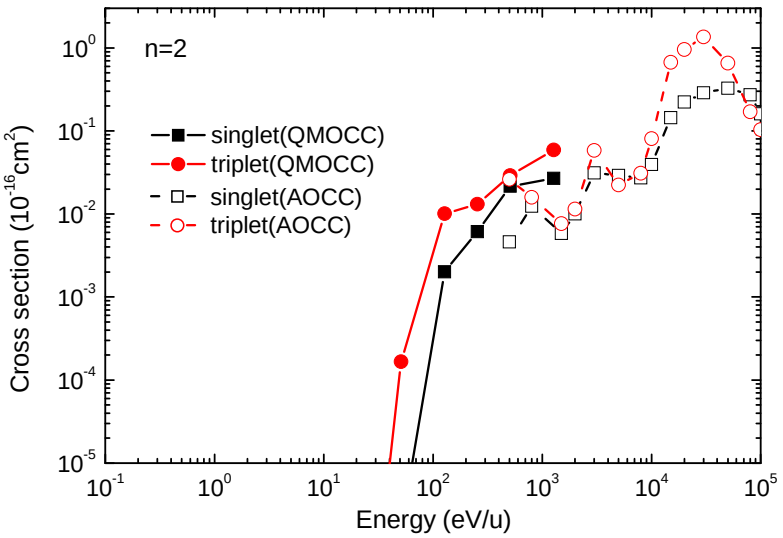

Fig. 11. (Color online) Cross sections for the electron capture to the n=2 shell singlet and triplet states of Be^{2+} ion.

B. 2*s*-2*p* excitation cross sections in Li

There are four states of $BeLi^{3+}$ molecular ion that asymptotically converge to the Be^{3+}+ Li(2p) dissociation products: $12^1\Sigma$, $11^3\Sigma$ and $7^{1,3}\Pi$ (see Table 1). The Σ states asymptotically converge to Li($2p_0$) state, while the Π states converge to the Li($2p_1$) state. The $12^1\Sigma$, $11^3\Sigma$ states are coupled by Landau-Zener radial couplings with the initial states $11^1\Sigma$ and $10^3\Sigma$, respectively, at the internuclear distance $4.5a_0$ (see Fig.3), that leads to population of Li($2p_0$) singlet and triplet states. The Li($2p_1$) singlet and triplet state are populated by the $12^1\Sigma$-$7^1\Pi$ and $11^3\Sigma$-$7^3\Pi$ rotational couplings. The relatively small internuclear distance at which the $11^1\Sigma$- $12^1\Sigma$ and $10^3\Sigma$-$11^3\Sigma$ couplings occur precludes large QMOCC 2*p* excitation cross sections. However, the small energy difference between the Li(2s) and Li(2p) states (1.848eV) ensures large TC- AOCC cross sections.

In Fig.12 we show the spin-resolved 2*p* excitation cross sections. In the entire energy range investigated the singlet and triplet cross sections are very close to each other. For the QMOCC cross sections the reason for this is the close magnitudes and positions of the radial $11^1\Sigma$- $12^1\Sigma$ and $10^3\Sigma$-$11^3\Sigma$ radial couplings that determine the flux along the singlet and triplet excitation channels. For the TC-AOCC cross sections this results from the fact that the excitation process is determined by the strengths of the couplings in the region of Li atom where the difference between singlet and triplet model potentials is very small. It should be noted that the common maximum of the spin-resolved 2*p* excitation cross sections is of the same order of magnitude as the spin-resolved total capture cross sections, except that it appears at a much higher collision energy.

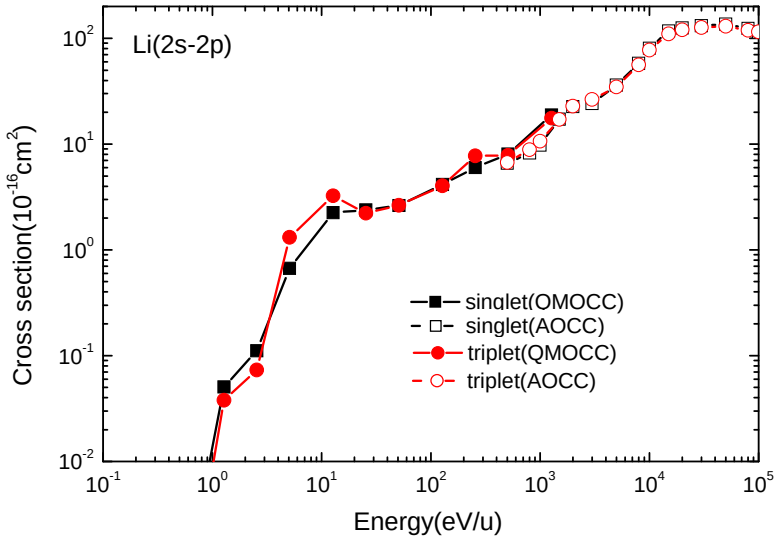

Fig. 12. (Color online) Spin-resolved and spin-averaged cross sections for excitation of Li($1s^2$2p) state in Be^{3+}-Li collisions.

V. CONCLUSIONS

In the present work, we have performed spin-resolved total and state-selective electron capture and Li(2s→2p) excitation cross section calcu-

lations in Be^{3+}-Li(2s) collisions by employing the QMOCC and TC-AOCC methods in the energy ranges 10^{-4}-1.2keV/u and 0.5-100keV/u, respectively. The molecular data used in the QMOCC calculations have been calculated by the *ab initio* MRDCI package, while spin-dependent one-particle model potentials were used in the TC-AOCC calculations. In the QMOCC calculations all Σ, Π, Δ and Φ molecular states of $BeLi^{3+}$ corresponding asymptotically to the $Be^{2+}(1snl)$ ($n \leq 4$)+Li^{+} and Be^{3+}+Li(2s, 2p) atomic states were included in the expansion basis. The expansion basis for the TC-AOCC calculations included all bound states with n≤4 centered on Li and all singlet and triplet bound states on Be^{3+} with $n \leq 10$ (l=0-5) plus 42 pseudostates for collision energies above 3keV/u, but for collision energies below 3keV/u the basis set centered on Be^{3+} ion was reduced to include only the bound states with $n \leq 9$ (l=0-5).

The calculations revealed that significant differences between the total singlet and triplet cross sections exist in the energy region below 0.1keV/u, while for higher energies the differences are negligible. Similar is the situation for the n=4 shell cross sections, except that the low energy singlet-triplet differences start already at 1keV/u. The differences between the singlet and triplet cross sections are particularly large for the 4l partial cross sections in the energy region below 1ke/u. In contrast, the differences between the spin-resolved 3l cross sections are significantly smaller and for the n=3 shell cross sections they are even smaller. Also, the singlet-triplet differences in the Li(2s→2p) excitation cross section are quite small. The origin of the differences (or their absence) between the singlet and triplet cross sections are discussed in terms of interstate couplings in the molecular and atomic description of the collision dynamics.

Acknowledgements

This work was supported by the Macedonian Academy of Sciences and Arts and by the National Basic Research Program of China (Grant No. 2013CB922200), and the National Natural Science Foundation of China (Grants No. 11474033, No. 11474032 and No. 11574326).

References

[1] R. K. Janev, L. P. Presnyakov, and V. P. Shevelko, *Physics of Highly Charged Ions* (Springer, Berlin-Heidelberg, 1985)

[2] K. McCormick, S. Fiedler, G. Kocsis, J. Schweinzer and S.Zoletnik, *Fusion Eng. Des.* **34**, 125 (1997)

[3] R. P. Schorn, E. Wolfrum, F. Aumayr, E. Hintz, D. Rusbüldt and H. Winter, *Nucl. Fusion* **32**, 351 (1992)

[4] R. P. Schorn, E. Hintz, D. Rusbüldt, F. Aumayr, M. Schneider, E. Unterreiter and H. P. Winter, *Appl. Phys. B* **52**, 71 (1991)

[5] M. Apicella, G. Mazzitelli, V. P. Ridolfini, V. Lazarev, A. Alekseyev, A. Vertkov and R. Zagorski, *J. Nucl. Mater.* **363**, 1346 (2007)

[6] E.L. Tabares, *Plasma Phys. Control. Fusion*, **58**, 014014 (2015)

[7] A. Loarte *et al*., *Nucl. Fusion* **47**, S203 (2007)

[8] R. J. Buenker and R. A. Phillips, *J. Mol. Struct.: THEOCHEM* 123, 291 (1985)

[9] S. Krebs and R. J. Buenker, *J. Chem. Phys.* **103**, 5613 (1995)

[10] W. Fritsch and C. D. Lin, *Phys. Rep*. **202**, 1 (1991)

[11] B. H. Bransden and M. R. C. McDowell, *Charge Exchange and the Theory of Ion-Atom Collisions* (Clarendon Press, Oxford, 1992)

[12] C. Bottcher, J. Phys. B 4, 1140 (1971)

[13] Yu. Ralchenko and A. E. Kramida, J. Reader, and NIST ASD Team, NIST Atomic Spectra Database (version 3.1.5), 2008; http://physics.nist.gov/asd3.

[14] L.F. Errea, F. Guzman, L. Mendez, B. Pons and A. Riera, *Phys. Rev. A* **77**, 012706 (2008)

[15] B. Zygelman, D. L. Cooper, M. J. Ford, A. Dalgarno, J. Gerratt and M. Raimondi, *Phys. Rev. A* **46**, 3846 (1992)

[16] M. Kimura and N. F. Lane, *Adv. At. Mol. Opt. Phys.* **26**, 79 (1990)

[17] B. R. Johnson, *J. Comput. Phys.* **13**, 445 (1973)

[18] T. G. Heil, S. E. Butler, and A. Dalgarno, *Phys. Rev. A* **23**, 1100 (1981)

[19] M. C. Bacchus-Montabonel and P. Ceyzeriat, *Phys. Rev. A* **58**, 1162 (1998)

[20] L. F. Errea, L. M´endez, and A. Riera, *J. Phys. B* **15**, 101 (1982)

[21] Dunning T. H. Jr, *J. Chem. Phys.* **90** 1007 (1989)

[22] L. F. Pacios and P. A. Christiansen, *J. Chem. Phys.* **82**, 2664 (1985)

[23] B. H. Bransden et al., *J. Phys. B* **17**, 4515 (1984)

[24] L. Liu, J. G. Wang and R. K. Janev, *J. Phys. B* **49**, 105201 (2016)

[25] J. L. Nolte, P.C, Stancil, H.P. Libermann, R.J. Buenker, Y. Hui and D.R. Schultz, *J. Phys. B* **45**, 245202 (2012)

[26] X.Y. Li, L. Liu, J. G. Wang and R. K. Janev, *J. Phys. B* **48**, 205205 (2015)

Содржина – Contents

Издавач:
Македонска академија на науките и уметноста – Скопје

Компјутерска обработка:
Драгица Топузоска

Печат:
„Винсент графика“ – Скопје

Тираж:
300 примероци

Бројот е излезен од печат во ноември 2018 година.